Characterization of Subthreshold Voltage Fluctuations in Neuronal Membranes

M. Rudolph
Michael.Rudolph@iaf.cnrs-gif.fr
A. Destexhe
Alain.Destexhe@iaf.cnrs-gif.fr
Unité de Neuroscience Intégratives et Computationnelles, CNRS,
91198 Gif-sur-Yvette, France

Synaptic noise due to intense network activity can have a significant impact on the electrophysiological properties of individual neurons. This is the case for the cerebral cortex, where ongoing activity leads to strong barrages of synaptic inputs, which act as the main source of synaptic noise affecting on neuronal dynamics. Here, we characterize the subthreshold behavior of neuronal models in which synaptic noise is represented by either additive or multiplicative noise, described by Ornstein-Uhlenbeck processes. We derive and solve the Fokker-Planck equation for this system, which describes the time evolution of the probability density function for the membrane potential. We obtain an analytic expression for the membrane potential distribution at steady state and compare this expression with the subthreshold activity obtained in Hodgkin-Huxley-type models with stochastic synaptic inputs. The differences between multiplicative and additive noise models suggest that multiplicative noise is adequate to describe the high-conductance states similar to in vivo conditions. Because the steady-state membrane potential distribution is easily obtained experimentally, this approach provides a possible method to estimate the mean and variance of synaptic conductances in real neurons.

1 Introduction

The investigation of dynamical systems in the presence of noise has received increasing attention. Phenomena like stochastic resonance (Benzi, Suter, & Vulpiani, 1981; Nicolis, 1982; for a review, see Gammaitoni, Hänggi, Jung, & Marchesoni, 1998) or noise-induced phase transitions (Horsthemke & Lefever, 1984; Van den Broeck, Parrondo, & Toral, 1994) show that in stochastic systems, qualitatively new behaviors can emerge, which in some cases can convey advantageous properties to the system. Especially in neural systems, which are found among the most natural examples of highly nonlinear excitable systems embedded in a noisy environment (Érdi, 1994;

Traynelis & Jaramillo, 1998; Longtin, 2000; Volgushev & Eysel, 2000; White, Rubinstein, & Kay, 2000), noise can have a profound impact on the dynamics on both the subthreshold level (Levitan, Segundo, Moore, & Perkel, 1968; Bernander, Douglas, Martin, & Koch, 1991; Rapp, Yarom, & Segev, 1992; Poznanski & Peiris, 1996; Doiron, Longtin, Berman, & Maler, 2000; Hillenbrand, 2002) and the superthreshold response (Poliakov, Powers, Sawczuk, & Binder, 1996; Gammaitoni et al., 1998; Hô & Destexhe, 2000; Tiesinga, José, & Sejnowski, 2000; Salinas & Sejnowski, 2000; Burkitt & Clark, 2001; Rudolph & Destexhe, 2001a, 2001b; Rudolph, Hô, & Destexhe, 2001).

Here we focus on neurons in the mammalian neocortex. In the cortical network, the ongoing spontaneous neuronal discharge activity in vivo acts as the main source of noise impinging on the behavior of individual neurons. Due to a very dense synaptic connectivity within this network, with each neuron receiving several thousand synaptic inputs from other neurons (Szentagothai, 1965; Cragg, 1967; Gruner, Hirsch, & Sotelo, 1974; DeFelipe & Fariñas, 1992), and high sustained firing rates up to 20 Hz on average for each neuron in awake animals (Hubel, 1959; Evarts, 1964; Steriade, 1978; Matsumura, Cope, & Fetz, 1988; Holmes & Woody, 1989; Steriade, Timofeev, & Grenier, 2001), cortical neurons are subject to a tremendous synaptic background noise (Calvin & Stevens, 1968; Contreras, Timofeev, & Steriade, 1996; Kohn, 1997; Nowak, Sanchez-Vives, & McCormick, 1997; Paré, Shink, Gaudreau, Destexhe, & Lang, 1998; Azouz & Gray, 1999; Lampl, Reichova, & Ferster, 1999). Intracellular recordings in conjunction with models of reconstructed cortical neurons show that the release at individual synaptic terminals during periods of intense spontaneous network activity can be described in leading order by a Poisson process (Cox & Lewis, 1966) with an average frequency of about 1 and 5 Hz for excitatory and inhibitory synapses, respectively (Destexhe & Paré, 1999). As it was shown in a number of experimental (Barrett, 1975; Holmes & Woody, 1989; Baranyi, Szente, & Woody, 1993a, 1993b; Borg-Graham, Monier, & Frégnac, 1998; Paré et al., 1998; Destexhe & Paré, 1999) and theoretical studies (Bernander et al., 1991; Rapp et al., 1992; Destexhe & Paré, 1999), this continuous strong barrage of synaptic inputs in vivo creates a highly fluctuating intracellular activity, characterized by a more depolarized membrane potential (V_m), persistent V_m fluctuations with higher amplitude, and a smaller membrane time constant (high-conductance state) compared to states without network activity (in vitro states).

To characterize the consequences of the sustained and intense background activity found in the cortical network in vivo on the neuronal dynamics and cellular response, various models of cortical neurons with components describing synaptic noise were constructed. These models cover a broad range of complexity, ranging from (leaky) integrate-and-fire neuron models (Lapicque, 1907) with gaussian white noise (Lánský & Lánská, 1987; Bindman, Meyer, & Prince, 1988; Tuckwell, 1988; Lánský & Rospars, 1995; Doiron et al., 2000; van Rossum, 2001; Brunel, Chance, Fourcaud, & Abbott,

2001), to stochastic membrane equations (Tuckwell & Walsh, 1983; Tuckwell, Wan, & Wong, 1984; Manwani & Koch, 1999a, 1999b; Tuckwell, Wan, & Rospars, 2002), up to biophysical-faithful models of single neurons in which synaptic background activity is incorporated by the random release at individual synaptic terminals according to Poisson processes (Bernander et al., 1991; Rapp et al., 1992; Lánský & Rodriguez, 1999; Manwani & Koch, 1999a, 1999b; Tiesinga et al., 2000; Rudolph & Destexhe, 2001a, 2001b; Rudolph et al., 2001; Tuckwell et al., 2002). As it was shown in Ricciardi and Sacerdote (1979), under point-like excitatory and inhibitory synaptic inputs Poisson-distributed in time, the neuron's membrane potential undergoes a continuous random walk. The latter is described by a temporally homogeneous Markov process obeying the governing Fokker-Planck equation for a dynamical random process of the Ornstein-Uhlenbeck (OU) type. Hence, the OU process, which describes low-pass filtered gaussian white noise and was originally introduced as a model of Brownian motion (Uhlenbeck & Ornstein, 1930; Wang & Uhlenbeck, 1945), belongs to the most prominent models for synaptic noise (Ricciardi & Sacerdote, 1979; Hänggi & Jung, 1994).

Recently it was shown (Destexhe, Rudolph, Fellous, & Sejnowski, 2001), using detailed biophysical models of cortical neurons subject to stochastic synaptic inputs, that the total conductance resulting from a sum of thousands of synaptic inputs has a power spectrum that approximates a Lorentzian (see Figure 1D; it is Lorentzian if the synaptic conductance decays as $\exp[-t/\tau]$), whose high-frequency limit follows a $1/f^2$ behavior, where f denotes frequency. The gaussian nature of the OU process and its Lorentzian spectrum qualitatively match the behavior of the conductances underlying synaptic noise for higher frequencies, thus providing an effective stochastic representation that captures the amplitude of the conductances, their standard deviation, and spectral structure. Moreover, the use of this effective representation in neocortical slices (Destexhe et al., 2001; Fellous, Rudolph, Destexhe, & Sejnowski, in press) successfully recreated the cellular properties typically found in the intact and activated brain. This further motivates the use of the OU process as a valid description of synaptic noise.

However, the complexity of the resulting stochastic equations allows us to address only specific problems analytically (e.g., statistical characteristics like mean and variance of the membrane potential; see Manwani & Koch, 1999a, 1999b; Tuckwell et al., 2002), whereas numerical methods (for a review, see Werner & Drummond, 1997) or approximations (e.g., mean-field approximation; see Van den Broeck, Parrondo, Armero, & Hernández-Machado, 1994; Ibañes, García-Ojalvo, Toral, & Sancho, 1999; Genovese & Muñoz, 1999) remain the standard tools. In addition, the particular mathematical form of noise terms and their incorporation into stochastic neuron models (i.e., the nature of the coupling of the noise to the neural system) are still the subject of controversy. Experimental results show that synaptic transmission underlies a voltage-dependent, and thus state-dependent, ki-

netics (Regehr & Stevens, 2001). This suggests that the synaptic current has to be described, according to Ohm's law, by a (possibly voltage-dependent) conductance term coupling multiplicatively to the state variable. In the case of random synaptic inputs, this would translate into a noisy conductance term with multiplicative coupling to the membrane potential (*multiplicative noise*). At leading order, however, the resulting noisy synaptic current can be described by a stochastic variable. In this case, the noise term due to synaptic background activity enters the equations governing the membrane potential time course in an additive way (*additive noise*; see, e.g., Kohn, 1997). Representing synaptic noise using an additive term yields a simpler mathematical description of stochastic neural systems and, thus, is the most commonly used model of synaptic noise dating back to the 1960s (Stein, 1967; for a recent study of additive noise described by an OU process, see Brunel et al., 2001). On the other hand, multiplicative noise appears to be more closely linked to biophysical dynamics. It is still debated to which extent the latter can faithfully reproduce neuronal dynamics in the presence of synaptic background activity (for a comparison between both noise couplings, see, e.g., Tiesinga et al., 2000).

In this article, we analyze neuronal models subject to both additive and multiplicative synaptic noise, with the aim of deriving an analytic description of the statistical properties of the membrane potential. The motivation for this approach is to understand the integrative properties of neurons in the presence of noise, as well as to provide methods to analyze experimental data. We compare models with additive (current-based) or multiplicative (conductance-based) synaptic noise described by Ornstein-Uhlenbeck processes (see appendix A). Using the Itô-Stratonovich calculus (van Kampen, 1981; Gardiner, 2002) and the Fokker-Planck approach (Risken, 1984), the resulting stochastic Langevin equation (Genovese & Muñoz, 1999) is solved, yielding an analytic expression for the steady-state membrane potential distribution in the presence of noise (see appendix B). The expressions obtained for additive and multiplicative noise are compared with numerical solutions of neuronal models with voltage-dependent currents for generating action potentials (Hodgkin-Huxley equations, see Hodgkin & Huxley, 1952). We provide a detailed comparison of additive (current-based) or multiplicative (conductance-based) models and delineate which models are most appropriate representations of the subthreshold dynamics in the presence of synaptic noise. We discuss possible applications for analyzing membrane potential distributions from experimental data.

2 Models of Cortical Neurons

Cortical neurons were described by the passive membrane equation,

$$C_m \frac{dV(t)}{dt} = -g_L \left(V(t) - E_L \right) - \frac{1}{a} I_{syn}(t), \tag{2.1}$$

where $V(t)$ denotes the membrane potential, C_m the specific membrane capacity, a the membrane area, g_L and E_L the leak conductance and reversal potential, respectively (Destexhe et al., 2001). The total synaptic current due to synaptic background activity $I_{syn}(t)$ was decomposed into a sum of three terms: two multiplicative noise terms, which describe noisy excitatory and inhibitory conductance components coupling multiplicatively to the membrane potential, $g_e(t)(V(t) - E_e)$ and $g_i(t)(V(t) - E_i)$, respectively, as well as an additive noise term, which describes a noisy current $I(t)$ (Stein, 1967; Ricciardi & Sacerdote, 1979):

$$I_{syn}(t) = g_e(t)(V(t) - E_e) + g_i(t)(V(t) - E_i) - I(t). \tag{2.2}$$

Here, $g_e(t)$ and $g_i(t)$ denote stochastic variables describing time-dependent excitatory and inhibitory conductances, respectively, and E_e and E_i are their respective reversal potentials.

The conductances $g_e(t)$ and $g_i(t)$ follow an OU process (Uhlenbeck & Ornstein, 1930; Wang & Uhlenbeck, 1945; see also section A.1), obeying

$$\frac{dg_{\{e,i\}}(t)}{dt} = -\frac{1}{\tau_{\{e,i\}}}(g_{\{e,i\}}(t) - g_{\{e,i\}0}) + \sqrt{D_{\{e,i\}}}\,\xi_{\{e,i\}}(t), \tag{2.3}$$

where $g_{\{e,i\}0}$ are the mean (static) excitatory and inhibitory conductances, $\tau_{\{e,i\}}$ are their corresponding time constants, and $D_{\{e,i\}}$ are the corresponding noise diffusion coefficients. Similarly, the additive current $I(t)$ is described by a single-variable OU process,

$$\frac{dI(t)}{dt} = -\frac{1}{\tau_I}(I(t) - I_0) + \sqrt{D_I}\,\xi_I(t), \tag{2.4}$$

where I_0 denotes the mean synaptic current, τ_I the current noise time constant, and D_I the corresponding noise diffusion coefficient. $\xi_{\{e,i\}}(t)$ as well as $\xi_I(t)$ denote independent gaussian white noise processes of zero mean $\langle \xi_{\{e,i,I\}}(t) \rangle = 0$ and unit standard deviation $\langle \xi_{\{e,i,I\}}(t)\xi_{\{e,i,I\}}(t') \rangle = \delta(t - t')$ for excitatory and inhibitory conductances, as well as the noisy current, respectively. White noise is obtained for vanishing time constants, whereas a time constant larger than zero yields "colored" gaussian noise for the corresponding process. The noise diffusion coefficients $D_{e,i}$ and D_I are related to the standard deviation $\sigma_{\{e,i\}}$ and σ_I of the respective stochastic variables by $\sigma_{\{e,i\}}^2 = \frac{1}{2}D_{\{e,i\}}\tau_{\{e,i\}}$ and $\sigma_I^2 = \frac{1}{2}D_I\tau_I$, respectively (see Gillespie, 1996). We note that the general form of the total synaptic current $I_{syn}(t)$, equation 2.2, contains both additive (current) and multiplicative (conductance) noise, which are commonly used as models to describe synaptic noise. As we will outline below, the explicit solution of this general model will allow us to investigate the effect of both noise couplings on the neuronal dynamics and to draw conclusions about their differences in more analytic terms.

Introducing the new variables $\tilde{g}_{\{e,i\}}(t) = g_{\{e,i\}}(t) - g_{\{e,i\}0}$ and $\tilde{I}(t) = I(t) - I_0$ yields for equation 2.1 the one-dimensional Langevin equation with two independent multiplicative and one additive Ornstein-Uhlenbeck noise terms,

$$\frac{dV(t)}{dt} = f(V(t)) + h_e(V(t))\,\tilde{g}_e(t) + h_i(V(t))\,\tilde{g}_i(t) + h_I\,\tilde{I}(t), \tag{2.5}$$

where $\tilde{g}_{\{e,i\}}(t)$ and $\tilde{I}(t)$ denote now stochastic variables with zero mean for excitatory conductance, inhibitory conductance, and the noisy current described by Ornstein-Uhlenbeck processes,

$$\frac{d\tilde{g}_{\{e,i\}}(t)}{dt} = -\frac{1}{\tau_{\{e,i\}}}\,\tilde{g}_{\{e,i\}}(t) + \sqrt{D_{\{e,i\}}}\,\xi_{\{e,i\}}(t), \tag{2.6a}$$

$$\frac{d\tilde{I}(t)}{dt} = -\frac{1}{\tau_I}\,\tilde{I}(t) + \sqrt{D_I}\,\xi_I(t), \tag{2.6b}$$

respectively. In equation 2.5, $f(V(t))$ denotes the $V(t)$-dependent drift term,

$$f(V(t)) = -\frac{g_L}{C_m}\,(V(t) - E_L) - \frac{g_{e0}}{C_m\,a}\,(V(t) - E_e)$$

$$-\frac{g_{i0}}{C_m\,a}\,(V(t) - E_i) + \frac{I_0}{C_m\,a}, \tag{2.7}$$

$h_{\{e,i\}}(V(t))$ voltage-dependent excitatory and inhibitory conductances noise terms, and h_I the current noise term:

$$h_{\{e,i\}}(V(t)) = -\frac{1}{C_m\,a}\,(V(t) - E_{\{e,i\}}), \tag{2.8a}$$

$$h_I = \frac{1}{C_m\,a}, \tag{2.8b}$$

respectively, which are nonanticipating functions of the membrane potential $V(t)$.

Equation 2.5 describes the subthreshold membrane potential dynamics in the presence of independent multiplicative and additive colored noise sources due to synaptic background activity. The stochastic terms prevent a direct analytic solution of this differential equation. However, the Itô-Stratonovich stochastic calculus (e.g., van Kampen, 1981; Gardiner, 2002) allows us to deduce the Fokker-Planck equation corresponding to the Langevin equation 2.5 and to describe the steady-state membrane potential probability distribution in the asymptotic limit $t \to \infty$ (details about the mathematical approach can be found in appendixes A and B). Briefly, in order to solve the Langevin equation 2.5, a set of differential rules (Itô rules) for the integrated OU process (see sections A.1 and A.2) is deduced (see section A.3).

Using the Itô rules, we obtain Itô's formula for the Langevin equation 2.5 in question (see section B.1). This formula describes the change of an arbitrary function for infinitesimal changes in its (stochastic) arguments. Averaging over Itô's formula finally yields the Fokker-Planck equation corresponding to equation 2.5 (see section B.2). For a general introduction to this approach, see Gardiner (2002).

3 The Steady-State Membrane Potential Probability Distribution

The Fokker-Planck equation, B.15,

$$
\begin{aligned}
\partial_t \rho(V, t) = &-\partial_V (f(V(t))\, \rho(V, t)) \\
&+ \partial_V (h_e(V(t))\, \partial_V (h_e(V(t))\, \alpha_e(t) \rho(V, t))) \\
&+ \partial_V (h_i(V(t))\, \partial_V (h_i(V(t))\, \alpha_i(t) \rho(V, t))) \\
&+ h_I^2\, \alpha_I(t)\, (\partial_V^2 \rho(V, t)),
\end{aligned}
\tag{3.1}
$$

where

$$
2\alpha_{\{e,i,I\}}(t) = \sigma_{\{e,i,I\}}^2\, \tau_{\{e,i,I\}} \left(1 - \exp\left[-\frac{t}{\tau_{\{e,i,I\}}}\right]\right)
$$

$$
+ \frac{1}{2\,\tau_{\{e,i,I\}}} \langle \tilde{w}_{\{e,i,I\}}^2(t) \rangle - \sigma_{\{e,i,I\}}^2\, t,
\tag{3.2}
$$

describes the time evolution of the probability $\rho(V, t)$ that the stochastic process, determined by the passive membrane equation 2.1, takes the value $V(t)$ at time t. We are interested in the steady-state probability distribution: $t \to \infty$. In this limit, $(\partial_t \rho(V, t)) \to 0$. To obtain explicit expressions for $\alpha_{\{e,i,I\}}(t)$, defined in equation 3.2, in the limit $t \to \infty$, we make use of the fact that for $t \to \infty$, the ratio $\frac{t}{\tau_{\{e,i,I\}}} \gg 1$. This leads to the assumption that in the steady state, the variables $\alpha_{\{e,i,I\}}(t)$ take a form corresponding to a Wiener process:

$$
\begin{aligned}
2\alpha_{\{e,i,I\}}(t) \xrightarrow[t\to\infty]{} &\ \sigma_{\{e,i,I\}}^2\, \tau_{\{e,i,I\}} \left(1 - \exp\left[-\frac{t}{\tau_{\{e,i,I\}}}\right]\right) \\
&+ \frac{1}{\tau_{\{e,i,I\}}} D_{\{e,i,I\}}\, t - \sigma_{\{e,i,I\}}^2\, t \\
= &\ \sigma_{\{e,i,I\}}^2\, \tau_{\{e,i,I\}}.
\end{aligned}
\tag{3.3}
$$

Here, relation A.12a with $D_{\{e,i,I\}} = \sigma_{\{e,i,I\}}^2\, \tau_{\{e,i,I\}}$ was used. The interpretation of equation 3.3 is that, in the limit $t \to \infty$, the noise correlation times $\tau_{\{e,i,I\}}$ become infinitesimally small compared to the time in which the steady-state probability distribution is obtained. In section 4, we will show that

this assumption indeed yields a steady-state probability distribution that closely matches that obtained from numerical simulations.

With equation 3.3, the Fokker-Planck equation 3.1 can be solved analytically, and we obtain the following steady-state probability distribution $\rho(V)$ for the membrane potential $V(t)$, described by the passive membrane equation 2.1 with two independent multiplicative and one additive colored (Ornstein-Uhlenbeck) noise sources:

$$\rho(V) = N \exp\left[\frac{a_1}{2\,b_2} \ln[b_2\,V^2 + b_1\,V + b_0] \right.$$

$$\left. + \frac{2\,b_2\,a_0 - a_1\,b_1}{b_2\,\sqrt{4\,b_2\,b_0 - b_1^2}} \arctan\left[\frac{2\,b_2\,V + b_1}{\sqrt{4\,b_2\,b_0 - b_1^2}} \right] \right], \quad (3.4)$$

where

$$a_0 = \frac{1}{(C_m\,a)^2}\,(2\,C_m\,a\,(g_L\,E_L\,a + g_{e0}\,E_e + g_{i0}\,E_i)$$

$$+ I_0\,C_m\,a + \sigma_e^2\,\tau_e\,E_e + \sigma_i^2\,\tau_i\,E_i),$$

$$a_1 = -\frac{1}{(C_m\,a)^2}\,(2\,C_m\,a\,(g_L\,a + g_{e0} + g_{i0}) + \sigma_e^2\,\tau_e + \sigma_i^2\,\tau_i),$$

$$b_0 = \frac{1}{(C_m\,a)^2}\,(\sigma_e^2\,\tau_e\,E_e^2 + \sigma_i^2\,\tau_i\,E_i^2 + \sigma_I^2\,\tau_I),$$

$$b_1 = -\frac{2}{(C_m\,a)^2}\,(\sigma_e^2\,\tau_e\,E_e + \sigma_i^2\,\tau_i\,E_i),$$

$$b_2 = \frac{1}{(C_m\,a)^2}\,(\sigma_e^2\,\tau_e + \sigma_i^2\,\tau_i), \quad (3.5)$$

and N is a normalization factor defined by $\int_{-\infty}^{\infty} dV\,\rho(V) = 1$.

Of particular interest are solutions of the stochastic passive membrane equation 2.1 with either multiplicative or additive noise only. Performing the limits $I_0 \to 0$ and $\sigma_I \to 0$ in equation 3.4 yields, in general, the asymmetric steady-state membrane potential distribution of the passive membrane equation subject to two independent colored multiplicative noise sources describing excitatory and inhibitory synaptic conductances:

$$\rho_{\text{mult}}(V) = N \exp\left[A_1 \ln\left[\frac{\sigma_e^2\,\tau_e}{(C_m\,a)^2}\,(V - E_e)^2 + \frac{\sigma_i^2\,\tau_i}{(C_m\,a)^2}\,(V - E_i)^2 \right] \right.$$

$$\left. + A_2 \arctan\left[\frac{\sigma_e^2\,\tau_e\,(V - E_e) + \sigma_i^2\,\tau_i\,(V - E_i)}{(E_e - E_i)\,\sqrt{\sigma_e^2\,\tau_e\,\sigma_i^2\,\tau_i}} \right] \right], \quad (3.6)$$

where

$$A_1 = -\frac{2\,a\,C_m\,(g_{e0} + g_{i0}) + 2\,a^2\,C_m\,g_L + \sigma_e^2\,\tau_e + \sigma_i^2\,\tau_i}{2\,(\sigma_e^2\,\tau_e + \sigma_i^2\,\tau_i)},$$

$$A_2 = \frac{\begin{aligned}2\,C_m\,a\,(a\,g_L\,(\sigma_e^2\,\tau_e\,(E_L - E_e) + \sigma_i^2\,\tau_i\,(E_L - E_i))\\ + (g_{e0}\,\sigma_i^2\,\tau_i - g_{i0}\,\sigma_e^2\,\tau_e)\,(E_e - E_i))\end{aligned}}{(E_e - E_i)\,\sqrt{\sigma_e^2\,\tau_e\,\sigma_i^2\,\tau_i}\,(\sigma_e^2\,\tau_e + \sigma_i^2\,\tau_i)}.$$

We note that due to the particular form of the membrane potential distribution $\rho_{\mathrm{mult}}(V)$ and the dependence of the coefficients (see equations 3.5) on the synaptic noise parameters, two different noise processes will, in general, not yield equivalent distributions.

Similarly, carefully performing the limits $g_{\{e,i\}0} \to 0$, $\sigma_{\{e,i\}} \to 0$ in equation 3.4 yields for the steady-state membrane potential distribution in the presence of colored additive (current) noise the gaussian

$$\rho_{\mathrm{add}}(V) = N_{\mathrm{add}}\,\exp\left[-\frac{(V - \overline{V})^2}{2\,\sigma_V^2}\right], \tag{3.7}$$

where $N_{\mathrm{add}} = \sqrt{\frac{g_L\,a^2\,C_m}{\pi\,\sigma_I^2\,\tau_I}}$ denotes the normalization constant and

$$\overline{V} = E_L + \frac{I_0}{g_L\,a}, \tag{3.8}$$

$$\sigma_V = \sqrt{\frac{\sigma_I^2\,\tau_I}{2\,a^2\,g_L\,C_m}} \tag{3.9}$$

denote the mean voltage and voltage standard deviation, respectively.

Interestingly, the noise time constants $\tau_{\{e,i,I\}}$ enter the expressions for the steady-state membrane potential distribution, equations 3.6 and 3.7, only in the combination $\sigma_{\{e,i,I\}}^2\,\tau_{\{e,i,I\}}$. This rather surprising result can be heuristically understood by looking at the nature of the effective stochastic processes. As it can be demonstrated in the framework of shot-noise processes, correlated activity among multiple synaptic input channels has an impact on the variance of the total conductance or current time course, which in the effective model is described by $\sigma_{\{e,i,I\}}^2$. On the other hand, nonzero noise time constants (which are linked to the kinetics of synaptic conductances or currents) result in an effective temporal correlation between individual synaptic events. Here, larger time constants yield larger temporal overlap between individual events, which contributes to a (temporal) correlation of the synaptic events. The latter will effectively yield an effect comparable to that of the correlation in the synaptic activity pattern, which is characterized by $\sigma_{\{e,i,I\}}$, thus providing a heuristic explanation of the strict coupling

between noise variance and time constant. This specific coupling also indicates that white noise sources with different "effective" variance $\sigma^2_{\{e,i,I\}} \tau_{\{e,i,I\}}$ could yield equivalent distributions. However, for more complex systems or different couplings (as in the case of voltage-dependent NMDA currents), this result will no longer hold.

Typical examples of membrane potential probability distributions resembling those found in activated states of the cortical network in vivo are shown in Figure 1 (gray traces in A, B, C), along with corresponding analytic distributions following from both additive and multiplicative synaptic noise models (black solid and dashed lines, respectively). Parameters in equations 3.6 and 3.7 were chosen to yield distributions that matched that obtained from the numerical solution of the passive membrane equation 2.1 (see Figure 1A), as well as those obtained from numerical simulations of a passive single-compartment model with thousands of excitatory and inhibitory synapses releasing according to independent Poisson processes (see Figure 1B) and of a detailed biophysical model of a morphologically reconstructed cortical neuron (see Figure 1C; e.g., Destexhe & Paré, 1999; Rudolph & Destexhe, 2001a, 2001b, 2003; Rudolph et al., 2001). The latter
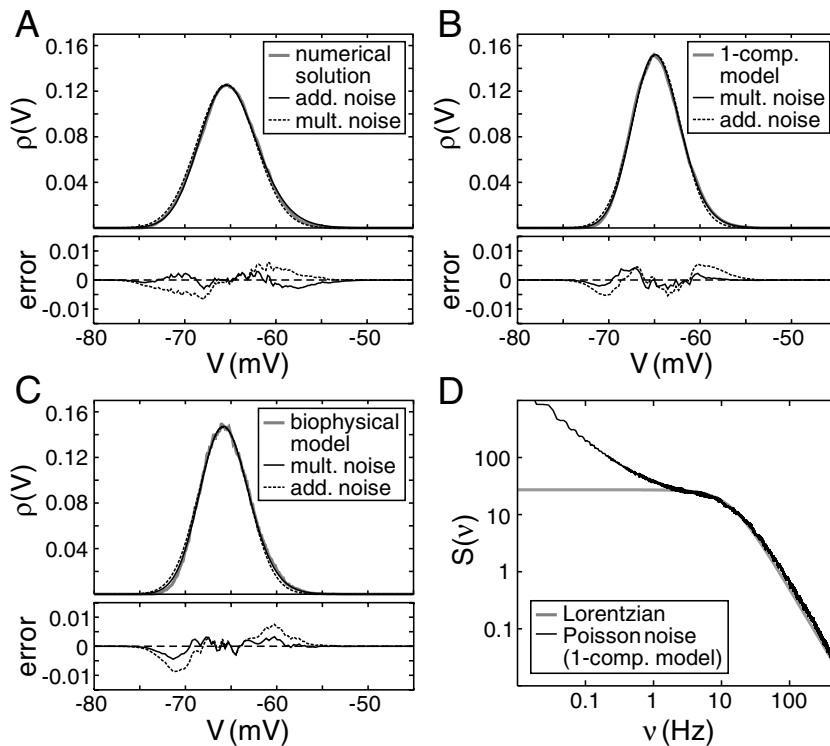
was shown to faithfully reproduce intracellular recordings obtained in vivo (see Destexhe & Paré, 1999).

These results indicate that the effective description of synaptic noise in terms of Ornstein-Uhlenbeck stochastic processes, along with the analytic solution of the corresponding stochastic membrane equation 2.1, provides a good description of the subthreshold activity of neuronal membranes in the presence of multiple synaptic inputs with biophysically more realistic kinetics (see Figures 1B and 1C). This motivates the use of equations 3.6 and 3.7 for characterizing synaptic activity in terms of conductance (or current) mean and standard deviation as the cause of subthreshold membrane potential fluctuations. Deviations were, in general, small but larger for the current noise description (see Figures 1B and 1C, bottom panels). Here, the error is primarily caused by the deviation of the power spectral density of the total conductance time course, stemming from a population of synaptic input channels, from a Lorentzian behavior (see Figure 1D) as well as the spatial

---

Figure 1: *Facing page*. Membrane potential probability distributions $\rho(V)$ for different models of synaptic noise. (A) Single-compartment model with two fluctuating synaptic conductances described by Ornstein-Uhlenbeck processes (see equation 2.1; for model parameter, see section 4). (B) Single-compartment model (see section 4 and Destexhe, Rudolph, Fellous, & Sejnowski, 2001), where synaptic activity was simulated by a large number of randomly releasing synapses. The 4472 excitatory and 3801 inhibitory synapses were described by kinetic models of AMPA and GABA$_A$ receptors (Destexhe et al., 1998), respectively, which released according to independent Poisson processes. (C) Compartmental model of cortical pyramidal neuron (morphologically reconstructed) in which synaptic activity was simulated by randomly-releasing synapses distributed in soma and dendrites (see the details of this model in Destexhe & Paré, 1999; Rudolph & Destexhe, 2003). In all cases shown in A–C, the membrane potential distributions (gray lines) closely matched the analytic solutions $\rho_{\mathrm{mult}}(V)$ for multiplicative and $\rho_{\mathrm{add}}(V)$ for additive noise (black solid and dashed lines, respectively; parameters: $g_{e0} = 0.0121\ \mu S$, $g_{i0} = 0.0573\ \mu S$, $\sigma_e = 0.006\ \mu S$, $\sigma_i = 0.0132\ \mu S$, $I_0 = 0.228$ nA, $\sigma_I = 0.165$ nA (A); $g_{e0} = 0.0127\ \mu S$, $g_{i0} = 0.0573\ \mu S$, $\sigma_e = 0.0049\ \mu S$, $\sigma_i = 0.0108\ \mu S$, $I_0 = 0.238$ nA, $\sigma_I = 0.137$ nA (B); $g_{e0} = 0.0148\ \mu S$, $g_{i0} = 0.0702\ \mu S$, $\sigma_e = 0.00696\ \mu S$, $\sigma_i = 0.0153\ \mu S$, $I_0 = 0.222$ nA, $\sigma_I = 0.142$ nA (C); in all cases: $\tau_e = 2.728$ ms, $\tau_i = 10.49$ ms, $\tau_I = 2$ ms). The deviation between numerical and analytical distributions (absolute error shown in the bottom panels of A–C) was in general larger when synaptic noise was described by additive (current) noise (for discussion, see section 5. (D) Typical example of the power spectral density $S(\nu)$ of conductances obtained from the single-compartment model of B (black). The latter yield nearly gaussian distributions, whose power spectral density (gray) matched the Lorentzian function $S(\nu) = \frac{2D\tau^2}{1+(2\pi\tau\nu)^2}$ (D is the diffusion coefficient, τ the noise time constant) expected for OU noise, for frequencies larger than ~ 1 Hz.

distribution of synaptic input channels (as for the case shown in Figure 1C). In contrast, deviations between the numerical solution of the passive membrane equation 2.1 and the corresponding analytic solutions (see Figure 1A) must primarily be attributed to statistical errors in the numerical solution (for discussion, see the next section).

4 Computational Models and Numerical Solutions

To assess the validity of the analytic solutions given by equations 3.6 and 3.7 and to investigate the error due to the incorporation of negative conductances as well as the impact of voltage-dependent membrane currents for generating action potentials, we constructed and numerically solved simplified single-compartment models of cortical neurons (Destexhe et al., 2001), described by either the passive membrane equation 2.1 (*passive model*) or the active membrane equation given by

$$C_m \frac{dV(t)}{dt} = -g_L \left(V(t) - E_L \right) - \sum_{int} I_{int}(t) - \frac{1}{a} I_{syn}(t) \tag{4.1}$$

(*active model*), where $\sum_{int} I_{int}(t)$ denotes the sum over intrinsic voltage-dependent currents, each of which was described by Hodgkin-Huxley models (Hodgkin & Huxley, 1952):

$$I_{int}(t) = \bar{g} \, m(t)^M h(t)^N \, (V(t) - E).$$

Here, $\bar{g}$ denotes the peak conductance density, E the reversal potential, $m(t)$ and $h(t)$ activation and inactivation variables for corresponding active currents, respectively. The present model included two voltage-dependent currents, a fast Na^+ current and a delayed-rectifier K^+ current, for action potential generation (Traub & Miles, 1991) with conductance densities of 8.4 mS/cm^2 and 7 mS/cm^2 (Huguenard, Hamill, & Prince, 1988), respectively. The membrane area of the compartment was $a = 34636 \, \mu m^2$, and passive parameters were $g_L = 0.0452$ mS/cm^2, $E_L = -80$ mV, $C_m = 1$ μF/cm^2 (Destexhe & Paré, 1999).

In the active model, equation 4.1, the synaptic current $I_{syn}(t)$ (see equation 2.2), was subject to the constraints $g_{\{e,i\}}(t) \geq 0$, $\forall t$, which are equivalent to a cutoff of unphysical negative excitatory and inhibitory conductances, whereas in the passive model (see equation 2.1), cases with and without cutoff were investigated. For both the active and passive models, two special cases were considered: $I(t) \equiv 0$, which yields multiplicative noise with the corresponding analytic solution described by equation 3.6, and $g_{\{e,i\}0}(t) \equiv 0$, yielding additive noise with the analytic solution given by equation 3.7. Standard background parameter values were chosen to obtain a spontaneous spiking activity of 3 to 4 Hz and an average membrane potential of -65 mV with standard deviation around 4 to 5 mV characteristic for in vivo

states of cortical neurons (Paré et al., 1998; Destexhe & Paré, 1999). For the model with multiplicative noise, corresponding standard background parameters were $E_e = 0$ mV, $E_i = -75$ mV, $g_{e0} = 0.0121$ μS, $g_{i0} = 0.0573$ μS, $\sigma_e = 0.012$ μS, $\sigma_i = 0.0264$ μS, $\tau_e = 2.728$ ms, and $\tau_i = 10.49$ ms. For the model with additive noise, standard values were $I_0 = 0.33$ nA, $\sigma_I = 0.33$ nA, and $\tau_I = 2.0$ ms. In most simulations, the synaptic background parameters were changed in a range between 0% and 260% relative to the standard values. This range covered the physiological range observed in vitro (average membrane voltage at rest $\overline{V} = -80$ mV, membrane voltage fluctuations with zero standard deviation σ_V, vanishing spontaneous firing rate ν) and in vivo ($\overline{V} \sim -65$ mV, 2 mV $\lesssim \sigma_V \lesssim 6$ mV, 1 Hz $\lesssim \nu \lesssim 20$ Hz).

First, we compared the steady-state membrane potential probability distribution for models with multiplicative and additive noise for two typical situations: a noisy resting state resembling low-conductance in vitro conditions ($g_{\{e,i\}0} = 0$, $I_0 = 0$; $\sigma_{\{e,i\}}$ and σ_I 10% of standard values; see Figures 2A and 3A) and a noisy depolarized state resembling in vivo conditions (Figures 2B and 3B). Close to rest, the analytic solution deviated markedly from the numerical solution of the passive membrane equation (with negative conductance cutoff) and the active membrane equation subject to multiplicative noise (see Figure 2A, gray and black dashed lines, respectively), whereas the error was comparably small for the passive model (see Figure 2A, solid gray line) as well as for the active and passive membrane equation subject to additive noise (see Figure 3A).

This strong deviation for multiplicative noise can be explained by the nature of the OU process and the multiplicative coupling of the stochastic conductance to the state variable $V(t)$. In the OU process, the conductance $g_{\{e,i\}}(t)$ fluctuates around a static value $g_{\{e,i\}0}$ with a gaussian distribution of standard deviation $\sigma_{\{e,i\}}$ (see Figure 4A). To allow for an analytic treatment, no restrictions were imposed on $g_{\{e,i\}0}$, $\sigma_{\{e,i\}}$ or their relative amplitudes. However, unless $g_{\{e,i\}0} \gg \sigma_{\{e,i\}}$, the stochastic conductances may take negative values and thus enter physically not meaningful parameter regimes (see Figure 4A, gray regions). These regimes, which were explicitly excluded in the passive model with negative conductance cutoff and the active case (see above), are especially pronounced in noisy low-conductance states where $g_{\{e,i\}0}$ is small compared to $\sigma_{\{e,i\}}$. The resulting rather sharp cutoff in $g_{\{e,i\}}(t)$ (see Figure 4A, dashed line) is responsible for a cutoff in the resulting membrane potential distribution (see Figure 4B, stars; see also Figure 2A, the gray dashed line). Due to the presence of independent excitatory and inhibitory stochastic conductances, two such cutoffs are present (at the hyperpolarized tail due to excitatory conductance cutoff and at the depolarized tail due to inhibitory conductance), leading to the typical deviation pattern shown in Figure 4C.

Despite this deviation caused by the limitations of the analytic approach (the explicit exclusion of negative conductances in equation 2.2 will lead to discontinuities and no longer allow solving equation 2.1 analytically), er-
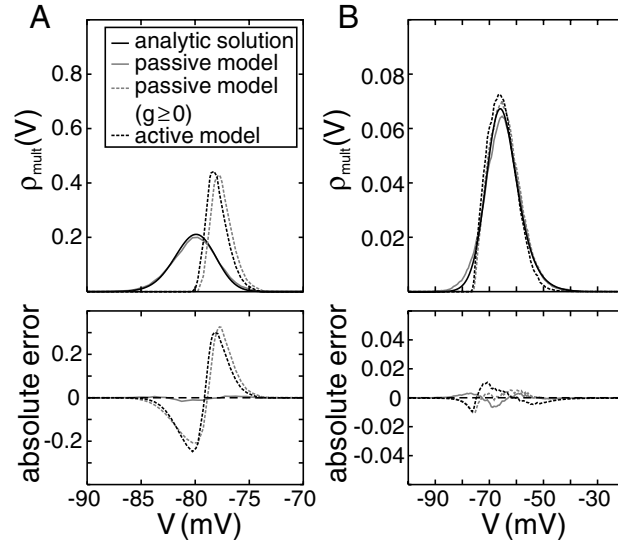
Figure 2: Examples of membrane potential probability distributions for multiplicative synaptic noise (conductance noise) $\rho_{\text{mult}}(V)$. Analytic solutions (black solid line) are compared to numerical solutions of the passive (gray solid line: without negative conductance cutoff; gray dashed line, with negative conductance cutoff) and an active (black dashed line) model (for model parameters, see section 4). (A) Low-conductance state around the resting potential, similar to in vitro conditions. (B) High-conductance state similar to in vivo conditions. The absolute error (bottom panels), defined as the difference between the numerical solution and the analytic solution, is markedly reduced in the high-conductance state. Model parameters were A $g_{e0} = 0$, $g_{i0} = 0$, $\sigma_e = 0.0012$ μS and $\sigma_i = 0.00264$ μS; B $g_{e0} = 0.0121$ μS, $g_{i0} = 0.0573$ μS, $\sigma_e = 0.012$ μS and $\sigma_i = 0.0264$ μS; for both: $\tau_e = 2.728$ ms and $\tau_i = 10.49$ ms.

rors in the numerical simulations contribute to deviations between the analytic and numerical result. Numerical integration of (nonlinear, coupled) stochastic differential equations crucially depends on the used integration procedure and integration time step. Here, larger time steps will make it more likely to encounter numerical instabilities. Moreover, although membrane potential distributions were characterized by first- and second-order moments only (i.e., mean and standard deviation, respectively), statistical errors due to limited simulation length are unavoidable. For numerical simulations, we used a temporal resolution of 0.1 ms and a simulation period of 100 s for each parameter setup. Simulations were performed using the NEURON simulation environment (Hines & Carnevale, 1997). We checked for numerical stability by running, for specific parameter setups, simulations with smaller integration time step (down to 0.01 ms) and longer integra-
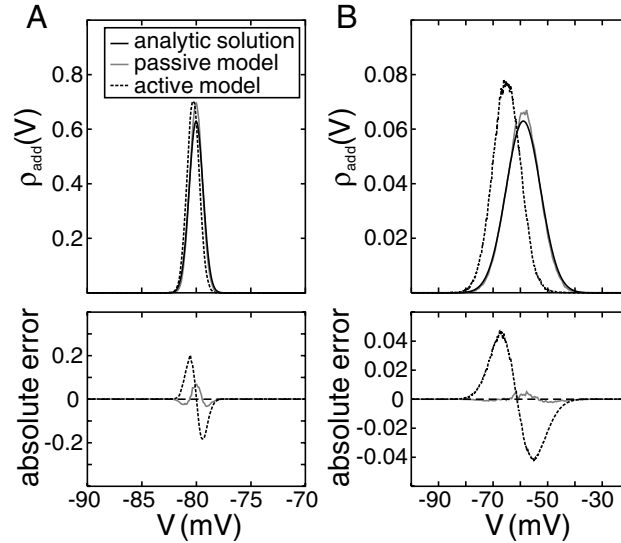
Figure 3: Examples of membrane potential probability distributions for additive synaptic noise (current noise) $\rho_{add}(V)$. Analytic solutions (black solid) are compared to the numerical solutions of the passive (gray solid line) and an active (black dashed line) model (for model parameters, see section 4). (A) Low-conductance state around the resting potential. (B) High-conductance state similar to in vivo conditions. The absolute error (bottom panels) is defined as the difference between the numerical solution and the analytic solution. The analytic solution gives a good description of the noisy resting state, whereas the contribution of voltage-dependent membrane currents in the active model yields a marked deviation in the in vivo state. Model parameters: $\tau_I = 2.0$ ms; $A\ I_0 = 0$, $\sigma_I = 0.033$ nA; $B\ I_0 = 0.33$ nA, $\sigma_I = 0.33$ nA.

tion periods (up to 500 s). In all cases, the mean and standard deviation converged slowly toward the analytic result (data not shown). However, the speed of this convergence depended on the parameters and was, for instance, much slower for situations in which either inhibition and excitation strongly dominated. Also, pronounced numerical instabilities were found for situations in which conductance fluctuations dominated over the mean conductance values and were especially present in the passive case without negative conductance cutoff.

However, for $g_{\{e,i\}0} \gtrsim \sigma_{\{e,i\}}$, which characterizes noisy high-conductance states resembling in vivo conditions, the impact of negative conductances and related numerical and statistical errors is expected to be small. Indeed, due to the smaller fraction of negative conductances (see Figure 4A, right), the error between the analytic and numerical solution is markedly reduced compared to resting conditions (see Figures 4B and 4C; see also Figure 2B, the
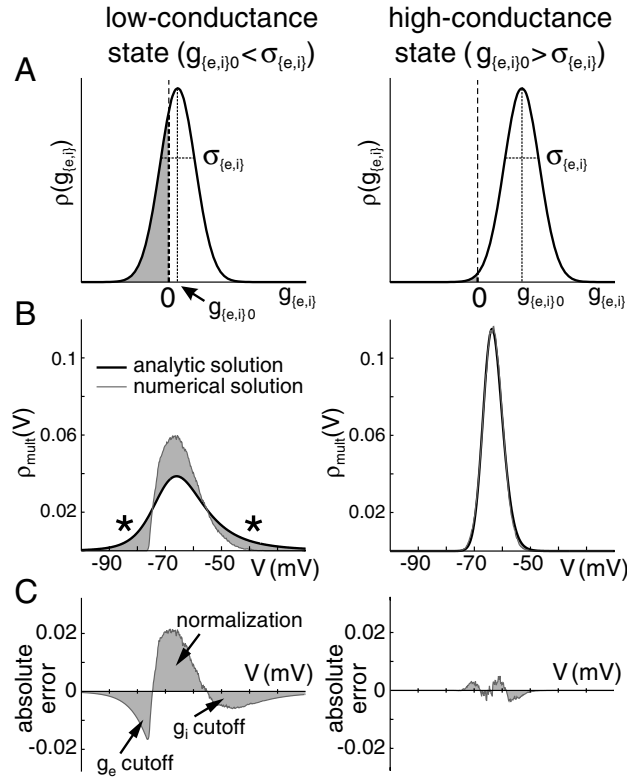
Figure 4: Contribution of negative conductances to the error between the analytic and numerical solution of the membrane potential probability distribution. Models with multiplicative synaptic noise $\rho_{\mathrm{mult}}(V)$ were considered in noisy low- and high-conductance states. The numerical solution was obtained for the passive model subject to the constraints $g_{\{e,i\}}(t) \geq 0$, $\forall t$. In low-conductance states with $g_{\{e,i\}0} < \sigma_{\{e,i\}}$, the nonzero probability $\rho(g_{\{e,i\}})$ for negative conductances (gray region in A; stochastic variable $g_{\{e,i\}}$ according to an Ornstein-Uhlenbeck noise process with mean $g_{\{e,i\}0}$ and standard deviation $\sigma_{\{e,i\}}$) yields membrane potential probability distributions with a pronounced tail for hyperpolarized and depolarized values due to excitatory and inhibitory conductances, respectively (B, stars). The gray regions in C show the corresponding absolute error, including the deviation due to normalization of the distributions. In noisy high-conductance states ($g_{\{e,i\}0} > \sigma_{\{e,i\}}$), the contribution of negative conductances and, thus, the error between analytic and numerical solution is only small.

gray dashed line). Moreover, the analytic membrane potential distribution also $\rho_{\text{mult}}(V)$ yields a good description for the active model (see Figure 2B, the black dashed line), suggesting that under high-conductance conditions, the conductance due to synaptic noise outlasts the conductance due to the (subthreshold) activity of voltage-dependent currents for spike generation, thus resulting in only a minor role of the latter in shaping the steady-state distribution.

In contrast, in the depolarized state typical for in vivo conditions, major differences were found between the analytical and the numerical solution of the active model for additive noise (see Figure 3B; compare the black dashed and solid lines). Here, the probability distribution for the active case is shifted toward the resting potential of the cell (i.e., hyperpolarized values), indicating a crucial role of active voltage-dependent currents by contributing nonnegligible conductances to the membrane under low-conductance conditions characteristic for models with additive noise.

5 Additive and Multiplicative Noise

Next, we characterized the parameter dependence of the mean $\overline{V}$ and standard deviation σ_V of the steady-state distribution. For multiplicative noise, the static components $g_{\{e,i\}0}$ were the main determinants of $\overline{V}$, with a nearly linear behavior of the iso-$\overline{V}$-lines as a function of $g_{\{e,i\}0}$ (see Figure 5A, left), leading to a shift of $\overline{V}$ toward the reversal potential for excitatory ($E_e = 0\,\text{mV}$) or inhibitory conductance ($E_i = -75$ mV) for increasing g_{e0} or g_{i0}, respectively. This behavior can be deduced from the analytic solution, equation 3.6, by calculating the maximum V_{max} of the probability distribution, which yields

$$\overline{V} \sim V_{\text{max}} = \frac{2\,C_m\,a\,(g_L\,E_L\,a + E_e\,g_{e0} + E_i\,g_{i0}) + \sigma_e^2\,\tau_e\,E_e + \sigma_i^2\,\tau_i\,E_i}{2\,C_m\,a\,(g_L\,a + g_{e0} + g_{i0}) + \sigma_e^2\,\tau_e + \sigma_i^2\,\tau_i} \qquad (5.1)$$

and approximates the mean $\overline{V}$. A qualitatively and quantitatively nearly identical behavior was found in the numerical solution of the passive model (compares Figures 5A and 5B, left; relative error between analytical and numerical solution < 0.5%). When negative conductances (see the discussion in section 4) were excluded (see equation 2.1 with constraint $g_{\{e,i\}}(t) \geq 0$, $\forall t$) and active voltage-dependent currents were incorporated (see equation 4.1), the mean $\overline{V}$ covered a smaller range of values (see Figure 6A and 6B, left, respectively). Especially for high excitatory mean conductances, the pronounced subthreshold activity of active membrane conductances acts against the depolarizing effect of excitation, thus effectively reducing $\overline{V}$ compared to models without active conductances. However, in the physiologically relevant parameter range (indicated by the convex regions in Figures 5 and 6), the error between the numerical solution of the active model and the analytic solution was smaller than 1 mV (relative error < 1.5%;
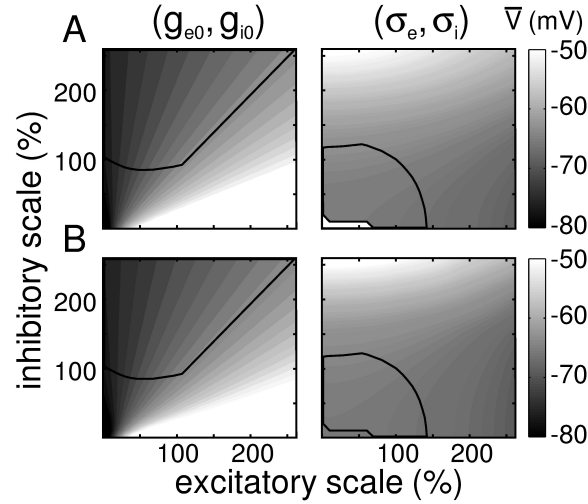
Figure 5: Mean of membrane potential probability distribution as a function of synaptic background parameters (left: $g_{\{e,i\}0}$, right: $\sigma_{\{e,i\}}$) for models with multiplicative noise. (A) The mean of the membrane potential probability distribution for the analytic solution, $\overline{V} = N \int_{-\infty}^{\infty} dV \, V \, \rho_{\text{mult}}(V)$, was obtained by numerical integration of equation 3.6. (B) Results for the numerical solution of the passive model (see equation 2.1) without negative conductance cutoff (for model parameters, see section 4). In all cases, corresponding excitatory and inhibitory background parameters were independently varied between 0% and 260% of the standard values, while the remaining ones were kept constant. The convex regions indicate the parameter range covering a cellular activity regime observed between the in vitro and in vivo state (see section 4).

compare Figures 5A and 6B, left). In the same parameter regime, the deviation of $\overline{V}$, obtained from the numerical integration of the passive model without negative conductances, and its analytic value did not exceed 1% (compare Figures 5A and 6A, left).

Equation 5.1 also shows a dependence of $\overline{V}$ on the standard deviations $\sigma_{\{e,i\}}$ of the stochastic conductances, with a shift to depolarized values for increasing σ_i (see Figure 5A, right). This effect was also observed in the numerical solution of the passive model (see Figure 5B, right), but only to much less of an extent in the passive model without negative conductances (see Figure 6B, right). No clear dependence was found in the active model (see Figure 6B, right). This suggests that this effect is a direct result of the presence of negative conductances for $\sigma_i > g_{i0}$. At $V(t)$ values larger than E_i, negative conductances effectively act like excitatory ones, causing a net depolarization of the membrane. However, in the physiological parameter range, $\overline{V}$ was nearly independent of $\sigma_{\{e,i\}}$, with an excellent agreement be-
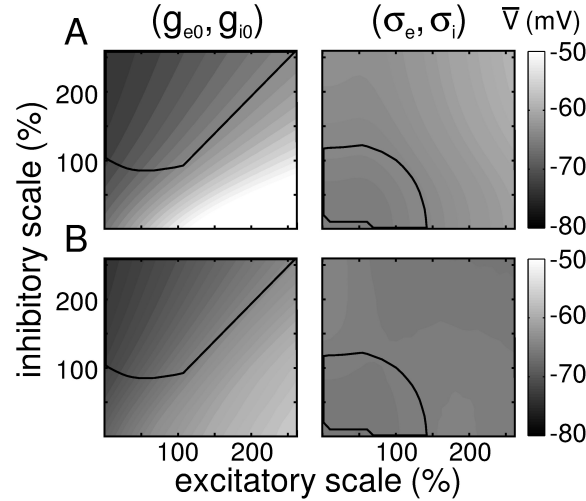
Figure 6: Mean of membrane potential probability distribution as a function of synaptic background parameters (left: $g_{\{e,i\}0}$, right: $\sigma_{\{e,i\}}$) for models with multiplicative noise. Results for the numerical solution of the (A) passive (equation 2.1; with negative conductance cutoff) and (B) active model (equation 4.1), respectively (for model parameters, see section 4). Corresponding excitatory and inhibitory background parameter were independently varied between 0% and 260% of the standard values, while the remaining ones were kept constant. The convex regions indicate the parameter range covering a cellular activity regime observed between the in vitro and in vivo state (see section 4).

tween numerical and analytic solution (relative error $< 0.5\%$, $< 0.75\%$ and $< 1.5\%$ for the passive model, the passive model without negative conductances, and the active model, respectively).

No analytic form of the standard deviation σ_V of the membrane potential distribution could be deduced from equation 3.6. However, numerical integration revealed a strong dependency of σ_V on both the static conductance components $g_{\{e,i\}0}$ and $\sigma_{\{e,i\}}$ (see Figure 7A). An increase in both σ_e and σ_i naturally leads to an increase in σ_V, whereas the impact of the mean conductances can be viewed as the result of two effects. First, the behavior of σ_V as a function of $g_{\{e,i\}0}$ follows closely that of $\overline{V}$ (compare Figures 5A and 7A, left panels), with a more depolarized membrane leading to a boosting of membrane potential fluctuations. Second, lower mean conductances yield a higher input resistance, which directly translates into an amplification of membrane potential fluctuations for fixed amplitude of input fluctuations. Due to the overall larger amplitudes of inhibition compared to excitation ($g_{i0} \sim 4.5\, g_{e0}$ and $\sigma_i \sim 2\, \sigma_e$ for the standard parameter values), σ_V was much more dependent on g_{i0} (see Figure 7A, left).
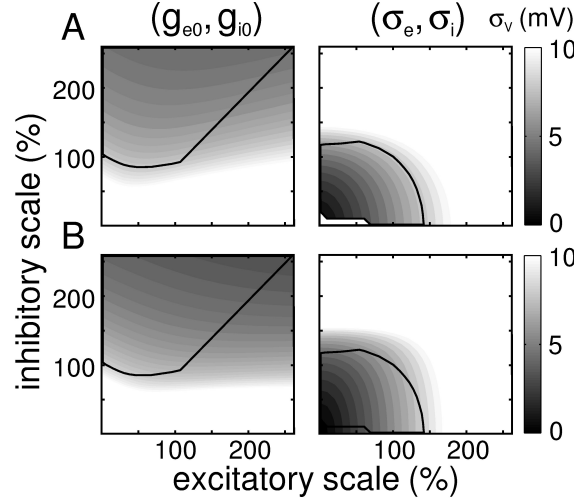
Figure 7: Standard deviation of membrane potential probability distribution as a function of synaptic background parameters (left: $g_{\{e,i\}0}$, right: $\sigma_{\{e,i\}}$) for models with multiplicative noise. (A) The standard deviation of the membrane potential probability distribution for the analytic solution, $\sigma_V^2 = N \int_{-\infty}^{\infty} dV\, (V - \overline{V})^2\, \rho_{\text{mult}}(V)$, was obtained by numerical integration of equation 3.6. (B) Results for the numerical solution of the passive model (equation 2.1) without negative conductance cutoff (for model parameters, see section 4). In all cases, corresponding excitatory and inhibitory background parameters were independently varied between 0% and 260% of the standard values, while the remaining ones were kept constant. The convex regions indicate the parameter range covering a cellular activity regime observed between the in vitro and in vivo state (section 4).

The numerical solution of the passive model (see Figure 7B, left) followed closely σ_V obtained from the analytic solution, with a relative error of less than 3% in the physiological parameter space, which is mostly attributable to numerical errors. The covered range of fluctuation amplitudes in the analytic solution and passive model was large (0 mV $< \sigma_V \lesssim$ 20 mV), but markedly decreased in the passive case without negative conductances (0 mV $< \sigma_V \lesssim$ 8 mV for changes in $g_{\{e,i\}0}$; 0 mV $< \sigma_V \lesssim$ 10 mV for changes in $\sigma_{\{e,i\}}$; see Figure 8A) and active model (0 mV $< \sigma_V \lesssim$ 7 mV for changes in $g_{\{e,i\}0}$; 0 mV $< \sigma_V \lesssim$ 8 mV for changes in $\sigma_{\{e,i\}}$; see Figure 8B). This indicates that negative conductance fluctuations have a boosting effect on the fluctuations of the membrane potential and that additional conductances due to the subthreshold activation of voltage-dependent currents effectively reduce the range of membrane potential fluctuations. However, despite the marked differences in the functional dependency of σ_V on $g_{\{e,i\}0}$ and $\sigma_{\{e,i\}}$,
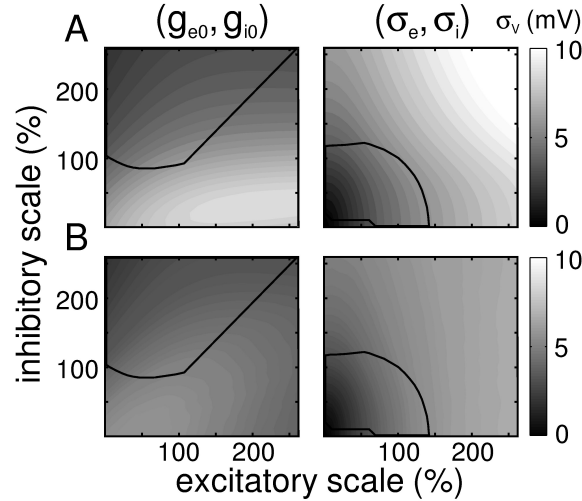
Figure 8: Standard deviation of membrane potential probability distribution as a function of synaptic background parameters (left: $g_{\{e,i\}0}$, right: $\sigma_{\{e,i\}}$) for models with multiplicative noise. Results for the numerical solution of the (A) passive (see equation 2.1; with negative conductance cutoff) and (B) active model (see equation 4.1), respectively (for model parameters see section 4). Corresponding excitatory and inhibitory background parameter were independently varied between 0% and 260% of the standard values, while the remaining ones were kept constant. The convex regions indicate the parameter range covering a cellular activity regime observed between the in vitro and in vivo state (see section 4).

in the physiological relevant parameter range, the absolute error between analytic and numerical solutions was smaller than 0.5 mV (relative error <8%).

Due to the strict coupling between $\sigma^2_{\{e,i\}}$ and the corresponding noise time constants $\tau_{\{e,i\}}$ (see equation 3.6 and section 3 for discussion), an impact of $\tau_{\{e,i\}}$ comparable to those of $\sigma_{\{e,i\}}$, but weaker in amplitude, on the mean and standard deviation of the membrane potential is expected. Indeed, even strong alterations of $\tau_{\{e,i\}}$ from its standard values only minimally changed $\overline{V}$ in the narrow range between -65 mV $\lesssim \overline{V} \lesssim -60$ mV (see Figure 9A, left). This result was confirmed by numerical simulations of the membrane equation 2.1 (see Figure 9A, right; relative error <0.8% in the physiological-relevant parameter range as indicated by the convex regions in Figure 9), as well as numerical stimulations of the passive model without negative conductances (relative error <1.0%) and the active model (relative error <1.5%).

The standard deviation of the membrane potential σ_V increased for both increasing excitatory and inhibitory time constants (Figure 9B, left) in a
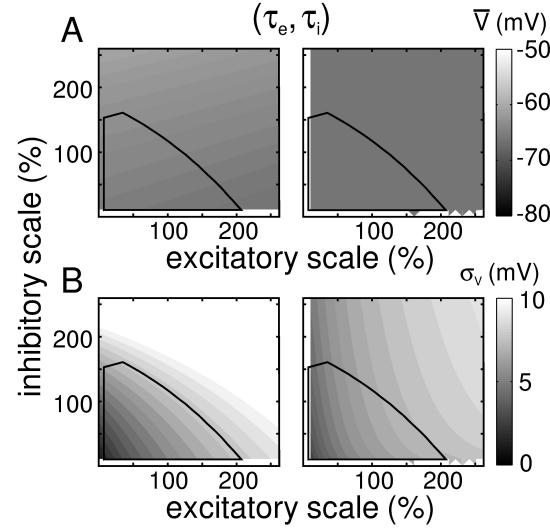
Figure 9: (A) Mean and (B) standard deviation of the membrane potential probability distribution as a function of conductance noise constants $\tau_{\{e,i\}0}$ for models with multiplicative noise. The left panels show the results for the analytic solution, with mean $\overline{V} = N \int_{-\infty}^{\infty} dV\, V\, \rho_{\mathrm{mult}}(V)$ and standard deviation $\sigma_V^2 = N \int_{-\infty}^{\infty} dV\, (V - \overline{V})^2\, \rho_{\mathrm{mult}}(V)$, obtained by numerical integration of equation 3.6. The right panels show the results for the numerical solution of the passive model (see equation 2.1) without negative conductance cutoff (for model parameters, see section 4). In all cases, corresponding excitatory and inhibitory noise time constants were independently varied between 0% and 260% of the standard values, while the remaining background parameters (conductance mean and variance) were kept constant. The convex regions indicate the parameter range covering a cellular activity regime observed between the in vitro and in vivo state (section 4).

fashion similar to those found for $\sigma_{\{e,i\}}$ (compare Figure 9B, left, and Figure 7A, right). However, it is interesting to note that only the analytic solution revealed, as expected, a marked effect of the conductance time constants. The increase of σ_V with increasing $\tau_{\{e,i\}}$ was less pronounced in the corresponding numerical solution of the passive membrane equation 3.6 (see Figure 9B, right; 0 mV $< \sigma_V \lesssim$ 9 mV compared to 0 mV $< \sigma_V \lesssim$ 14 mV in the analytic case for a corresponding parameter range), the passive model without negative conductances and the active case (0 mV $< \sigma_V \lesssim$ 6 mV in both cases; data not shown). This deviation between analytic and numerical results can primarily be assigned to the limits of the numerical simulations, where instabilities in the integration of the stochastic differential equation 3.6 were found to be present especially at long noise time constants. The deviations also reveal the limit of the analytic approach, especially of as-
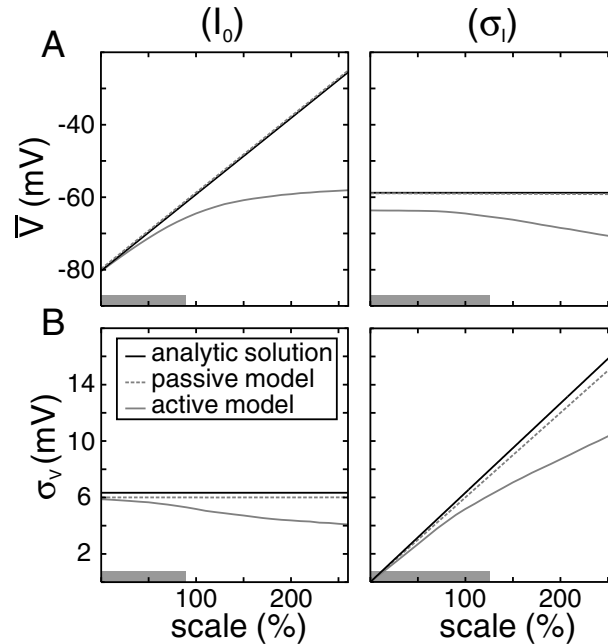
Figure 10: Mean and standard deviation of the membrane potential probability distribution as functions of synaptic background parameters for models with additive noise. The (A) mean $\overline{V}$ and the (B) standard deviation σ_V, which are respectively described by equations 3.8 and 3.9, are shown as functions of the synaptic background parameters (left: I_0; right: σ_I). Results for the analytic solution (black solid line) and the active (gray solid line) and passive (gray dashed line) models are shown (for model parameters see section 4). Background parameters were varied between 0% and 260% of the standard values. The gray bars indicate the parameter range covering a cellular activity regime observed between the in vitro and in vivo state (see section 4).

sumption 3.3. However, in the physiological-relevant parameter range, the error did not exceed that found for $\sigma_{\{e,i\}}$ (see above).

In contrast to the multiplicative noise case, the gaussian shape of the analytic solution for additive noise, equation 3.7, yields explicit expressions for the mean and standard deviation of the steady-state membrane potential distributions, equations 3.8 and 3.9, respectively. Here, a linear increase of $\overline{V}$ with increasing mean background current I_0 is expected, whereas the average membrane potential is independent of σ_I. The opposite functional dependency should be observed for σ_V, with σ_V proportional to σ_I but independent of I_0 (see Figure 10, solid lines). The numerical solution of the passive membrane equation closely follows this behavior (compare the black

solid and gray dashed lines in Figure 10), suggesting that additive noise yields a valid description of synaptic noise for passive models without additional conductances.

However, the presence of active channels led to a marked deviation from the analytic or passive solution (see Figure 10, the gray solid line) for both $\overline{V}$ and σ_V, with relative errors in the physiological-relevant parameter range of about 7.5% in $\overline{V}$, as well as 20% and 40% in σ_V for changes of I_0 and σ_I, respectively. These strong deviations can be attributed to the subthreshold activity of the voltage-dependent currents included for spike generation, which contribute a not negligible amount of conductance compared to the membrane (leak) conductance in the passive models with additive noise. This indicates that models of low conductance states, in which synaptic noise is incorporated by additive coupling, are less suitable for describing membrane activity in the presence of voltage-dependent currents under in vivo conditions.

6 Discussion

To characterize the subthreshold dynamics of neurons in the presence of synaptic noise, we studied the stochastic passive membrane equation subject to two independent multiplicative (conductance) noise sources as well as additive (current) noise (see equation 2.1). We deduced the Fokker-Planck equation for this system and obtained analytic expressions for the steady-state membrane potential probability distribution. We then used this analytic solution to compare current-based (additive noise) and conductance-based (multiplicative noise) models. The analytic solution can be used to investigate the link between subthreshold and superthreshold activity. It may also provide a novel method to estimate the mean and variance of synaptic conductances from experimental data. We discuss these points below.

6.1 A Characterization of Subthreshold Activity. The Fokker-Planck equation describes the time evolution of the probability density function for the membrane potential. This approach was applied in several previous studies (e.g., Ricciardi & Sacerdote, 1979; De Groff, Neelakanta, Sudhakar, & Aalo, 1993) aiming at the characterization of subthreshold activity in various neuronal models in the presence of noise (e.g., Levitan et al., 1968; Rapp et al., 1992; Poznanski & Peiris, 1996; Hillenbrand, 2002). However, most of these previous studies have considered additive noise sources, which yield a valid description only for low-conductance states (see below). Cortical neurons in vivo are in a high-conductance state (Borg-Graham et al., 1998; Paré et al., 1998; Destexhe & Paré, 1999), which is more appropriately described by conductance-based noise models (Destexhe et al., 2001). However, these conductance-based models are equivalent to multiplicative noise, which substantially limits the solubility of the governing stochastic equations.

An interesting comparison between both types of models was proposed recently (Lánský, Sacerdote, & Tomassetti, 1995). There, a conductance-based model (the Feller model) was described by a diffusion equation with an inhibitory reversal potential, which can be transformed into the standard form of a Feller process (Feller, 1951) by using the space transformation for diffusion processes. The Feller model, which is equivalent to a reduced version (no state dependent stochastic process for excitation) of our passive model with multiplicative noise (see equation 2.1), was compared with a current-based model (the OU model), which corresponds to the model subject to additive synaptic noise used here. As correctly argued, the introduction of a state-dependent infinitesimal mean and variance of the stochastic process, hence the Feller model, should yield a better description of the behavior of real neurons.

The equations we used here included both additive and multiplicative noise sources and are therefore general (they include the above models as particular cases). We provided the Fokker-Planck equation for such a system and showed that an analytic solution can be obtained at steady state. This steady-state membrane potential distribution is expressed in terms of the parameters of the synaptic noise (the mean excitatory and inhibitory conductances, their respective standard deviations, and time constants). These quantities can be compared to numerical simulations or to experimental data (see below).

To validate our approach, we compared the analytic solution of the steady-state membrane potential distribution to cases of increasing complexity. In a first step, the analytic solution was tested against numerical simulation of the passive membrane equation with two multiplicative or one additive OU noise sources (see Figure 1A). The quasi-perfect correspondence between the two models (compare Figures 5A and 5B, Figures 7A and 7B, and Figure 10, the black and gray dashed lines) validates the obtained analytic solution for $\rho(V)$. We further tested the analytic solution using single-compartment models receiving thousands of random synaptic inputs simulated by conductance-based kinetic models (see Figures 1B and 1D; see Destexhe et al., 2001), as well as by using multicompartment model of a neocortical pyramidal neuron with distributed synaptic inputs in its dendrites (see Figure 1C). In all cases, the analytic solution was in excellent agreement with the membrane potential distributions obtained numerically using the same parameters for synaptic conductances.

One possible drawback of this approach is that the presence of voltage-dependent currents may induce significant deformations of the voltage distribution. We tested this aspect by including voltage-dependent conductances for action potentials as well as spike-frequency adaptation (see section 4). Because the membrane potential operates mainly in the subthreshold regime and due to the high conductance of synaptic currents, the deviations due to voltage-dependent currents were found to be minor in conductance-based models (see Figure 2B). However, in current-based models, these

deviations were significant, especially in the region near threshold (see Figure 3B), suggesting that this type of model is less appropriate for analyzing subthreshold activity (see below).

6.2 Comparison Between Current-Based and Conductance-Based Models. In current-based models of synaptic noise, the additive coupling to the state variable $V(t)$ yields a symmetric gaussian probability distribution (see equation 3.7). In conductance-based models, the multiplicative coupling yields a membrane potential distribution that in general is asymmetric (see equation 3.6), due to the presence of reversal potentials. As discussed above, conductance-based models provide a reasonably accurate description of distributions obtained from numerical solutions of biophysical models in conditions of intense synaptic activity (e.g., see Figure 1C), and the contribution of voltage-dependent conductances of spike generation was minor in the subthreshold voltage range. This was not the case for current-based models, because in this case, the low conductance of the membrane is significantly contaminated by voltage-dependent currents, even in the subthreshold range. As a consequence, the current-based analytic distributions do not approximate well that of models containing voltage-dependent currents. Furthermore, the high-conductance state caused by the multiplicative coupling of the noise to the state variable $V(t)$ effectively diminished the impact of fluctuations on the intracellular activity, resulting in a larger bandwidth of changes in the network activity, which could modulate the electrophysiological dynamics and response of individual neurons in a physiologically meaningful range. The conductance-based (multiplicative noise) models therefore provide a better description of synaptic noise in conditions of intense activity resembling in vivo conditions.

However, conductance-based models of synaptic background activity deviated markedly from the numerical solution for low-activity states resembling in vitro conditions. Although the numerical solution of the passive model was in excellent agreement with the analytic solution, the presence of reversal potentials for excitatory and inhibitory synaptic conductances, as well as the cutoff of physically not meaningful negative conductances in the numerical integration of the active model, led to strong deformations of the steady-state membrane potential distribution compared to the analytic distribution obtained for equivalent parameters. This suggests that the present analytic model with noisy conductances is less suitable for the description of noisy low-conductance states (in vitro–like states), in which case models with additive noise would be more appropriate. In agreement with previous findings (Lánský et al., 1995; see the discussion above), our results suggest that conductance-based (multiplicative noise) models yield a better description of synaptic noise in neurons.

6.3 Possible Extensions of the Model. A possible extension of our approach could be to refine the model to account for the cutoff of negative

conductances or additional conductances related to spike-generating mechanisms. The typical shape of the emerging error (see Figure 4C, left) is determined by the relative amplitude of excitatory and inhibitory conductances, as well as the value of the mean membrane potential with respect to the reversal potentials of excitation and inhibition. A heuristically deduced voltage-dependent correction term could be included in the normalization term N in $\rho_{mult}(V)$, equation 3.7, in order to compensate the effect of negative conductances. In addition, although the functional form of Hodgkin-Huxley-based voltage-dependent conductances for spike generation does not allow an explicit solution of the active model described by the membrane equation 4.1, linearized conductance-based models (Mauro, Conti, Dodge, & Schor, 1970; Koch, 1999) could be used to capture the subthreshold activity of active conductances and thus may allow an analytic approach to the biophysically more realistic situation of an active membrane subject to multiplicative noise.

Another extension would be to use the solution of the steady-state membrane potential distribution, equation 3.4, to access the link between subthreshold and superthreshold activity, and to investigate the dependence of the cellular response on various background parameters (for a related study, see Salinas & Sejnowski, 2000). Experiments and numerical simulations suggest that the mean excitatory and inhibitory conductances determine the average firing rate, thus, the "working point" of the cell, whereas the statistics of the synaptic background activity, characterized by the standard deviation of the excitatory and inhibitory noise components, preferably has an impact on changes of the firing rate, thus the "sensitivity" (or gain) of the cell to changes in the synaptic inputs (Hô & Destexhe, 2000; Chance, Abbott, & Reyes, 2002; Rudolph & Destexhe, 2002; Prescott & De Koninck, 2003; Fellous et al., in press). If a link between subthreshold activity and cellular response could be established (see, e.g., Koch, Bernander, & Douglas, 1995), this modulating effect of the cellular gain by synaptic network activity could be formulated and investigated in more analytic terms.

Finally, the expressions obtained here could be used as a basis to analyze experimental data. The analytic expressions given in equations 3.6 and 3.7 could be fit to distributions obtained from intracellular recordings in vivo, yielding an estimate of the average excitatory and inhibitory synaptic conductances, as well as their variance. This procedure would allow estimating the statistical properties of excitatory and inhibitory conductances during different states of the network, or during responses to stimuli. Furthermore, this approach would also allow confining the parameters for experiments that aim at recreating in vivo activity in in vitro slice preparations (Destexhe et al., 2001; Fellous et al., in press). However, this procedure relies on the assumption that the experimental data are collected in a region of the membrane potential where there is little contamination from voltage-dependent currents. The evaluation of this method from experimental data and the assessment of its sensitivity will be the subject of a forthcoming study.

A: The Integrated Ornstein-Uhlenbeck Process ―――――――

In this appendix, we briefly review basic properties of the OU and the integrated OU stochastic process. The latter will be used for solving the Langevin equation 2.5. In particular, the Itô rules for the integrated OU process are presented (see equations A.13), which allow deducing Itô's formula and the Fokker-Planck equation (see equations B.10 and 3.1 in appendix 6.3, respectively) for the Langevin equation in question.

A.1 The Ornstein-Uhlenbeck Stochastic Process. The Ornstein-Uhlenbeck stochastic process is a special example of a Markov process, which describes a stochastic variable $\tilde{v}(t)$ with the unconditional and conditional probability distributions

$$\rho(\tilde{v}, t) = \frac{1}{\sqrt{2\pi\,\sigma^2}} \, \exp\left[-\frac{\tilde{v}^2(t)}{2\,\sigma^2}\right], \tag{A.1a}$$

$$\rho(\tilde{v}, t_1 \mid \tilde{v}, t_0) = \frac{1}{\sqrt{2\pi\,S^2}} \, \exp\left[-\frac{1}{2\,S^2}(\tilde{v}(t_1) - \tilde{v}(t_0)\,e^{-\frac{\Delta t}{\tau}})^2\right], \tag{A.1b}$$

where $\Delta t = |t_1 - t_0|$, τ denotes the correlation time and $S^2 = \sigma^2\,(1 - e^{-\frac{2\Delta t}{\tau}})$. The OU process is homogeneous in time ($\rho(\tilde{v}, t_1 \mid \tilde{v}, t_0)$ depends only on Δt) and stationary; $\rho(\tilde{v}, t)$ does not change in time. The corresponding characteristic functions, defined as the Fourier transforms of the probability distributions, are given by

$$G_{\tilde{v}}(s, t) = \exp\left[-\frac{\sigma^2}{2}\,s^2\right], \tag{A.2a}$$

$$G_{\tilde{v}}(s_0, t_0; s_1, t_1) = \exp\left[-\frac{\sigma^2}{2}\,(s_0^2 + s_1^2 + 2s_0 s_1\,e^{-\frac{\Delta t}{\tau}})\right], \tag{A.2b}$$

respectively. The associated one-dimensional moments $\langle \tilde{v}^n(t) \rangle$ and multidimensional moments $\langle \tilde{v}^{n_0}(t_0)\,\tilde{v}^{n_1}(t_1) \rangle$, defined as the coefficients in the Taylor expansion of the characteristic functions A.2, respectively, are

$$\langle \tilde{v}^n(t) \rangle = \begin{cases} 0 & \text{for odd } n, \\ \frac{(2k)!}{k!}\,\left(\frac{\sigma^2}{2}\right)^k & \text{for even } n = 2k, \end{cases} \tag{A.3a}$$

$$\langle \tilde{v}^{n_0}(t_0)\,\tilde{v}^{n_1}(t_1) \rangle = \begin{cases} 0 & \text{for odd } (n_0 + n_1), \\ \sigma^2\,e^{-\frac{\Delta t}{\tau}} & \text{for } n_0 = 1,\ n_1 = 1, \\ 3\sigma^4\,e^{-\frac{\Delta t}{\tau}} & \text{for } n_0 = 3,\ n_1 = 1, \\ \sigma^4\,(1 + e^{-\frac{2\Delta t}{\tau}}) & \text{for } n_0 = 2,\ n_1 = 2. \\ \dots. \end{cases} \tag{A.3b}$$

The logarithms of equations A.2 define the one-dimensional and multidimensional cumulants $\langle\langle\tilde{v}^n(t)\rangle\rangle$ and $\langle\langle\tilde{v}^{n_0}(t_0)\,\tilde{v}^{n_1}(t_1)\rangle\rangle$, respectively:

$$\langle\langle\tilde{v}^n(t)\rangle\rangle = \begin{cases} \sigma^2 & \text{for } n = 2, \\ 0 & \text{otherwise,} \end{cases} \tag{A.4a}$$

$$\langle\langle\tilde{v}^{n_0}(t_0)\,\tilde{v}^{n_1}(t_1)\rangle\rangle = \begin{cases} \sigma^2 e^{-\frac{\Delta t}{\tau}} & \text{for } n_0 = n_1 = 1, \\ 0 & \text{otherwise for } n_0,\,n_1 \neq 0. \end{cases} \tag{A.4b}$$

A straightforward calculation shows that moments and cumulants are related to each other by the following expression:

$$\langle\langle\tilde{v}^n(t)\rangle\rangle = n! \sum_{i=1}^{n} \sum_{k_1,\ldots,k_n} (-1)^{i-1}\,(i-1)! \prod_{m=1}^{n} \frac{1}{k_m!} \left(\frac{\langle\tilde{v}^m(t)\rangle}{m!} \right)^{k_m}. \tag{A.5}$$

Here, the second sum runs over all n-tuple $(k_1,\ldots,k_n)$ for which $\sum_{m=1}^{n} m\,k_m = n$, $\sum_{m=1}^{n} k_m = i$. Similarly, for the multidimensional moments and cumulants, one can prove the relation

$$\langle\langle\tilde{v}^{n_0}(t_0)\,\tilde{v}^{n_1}(t_1)\rangle\rangle = n_0!\,n_1! \sum_{i=1}^{n_0+n_1} \sum_{k_{(l,m)}} (-1)^{i-1}\,(i-1)!$$

$$\times \prod_{l,m}^{n} \frac{1}{k_{(l,m)}!} \left(\frac{\langle\tilde{v}^l(t_0)\tilde{v}^m(t_1)\rangle}{l!\,m!} \right)^{k_{(l,m)}}, \tag{A.6}$$

where the second sum denotes the sum over all (l,m)-tuple $k_{(l,m)}$ for which

$$\sum_{\substack{m=0 \\ }}^{n_1} \sum_{\substack{l=0 \\ l+m \geq 1}}^{n_0} k_{(l,m)}\,l = n_0\,,$$

$$\sum_{\substack{m=0 \\ }}^{n_1} \sum_{\substack{l=0 \\ l+m \geq 1}}^{n_0} k_{(l,m)}\,m = n_1\,,$$

$$\sum_{m=0}^{n_1} \sum_{l=0}^{n_0} k_{(l,m)} = i\,.$$

A.2   The Integrated Ornstein-Uhlenbeck Stochastic Process. In order to solve the Langevin equation 2.5, the stochastic variables $\tilde{g}_{\{e,i\}}(t)$ and $\tilde{I}(t)$ need to be integrated. To that end, we formally define the integrated OU

process,

$$\tilde{w}(t) = \int_0^t d\tilde{w}(s) = \int_0^t ds\, \tilde{v}(s), \tag{A.7}$$

of an OU stochastic process $\tilde{v}(t)$.

A straightforward calculation shows that the cumulants of $\tilde{w}(t)$ are given by

$$\langle\langle \tilde{w}^n(t) \rangle\rangle = \begin{cases} 2\sigma^2\,\tau\,t - 2\sigma^2\,\tau^2(1 - e^{-\frac{t}{\tau}}) & \text{for } n = 2, \\[2mm] 0 & \text{otherwise,} \end{cases} \tag{A.8a}$$

$$\langle\langle \tilde{w}^{n_0}(t_0)\tilde{w}^{n_1}(t_1) \rangle\rangle = \begin{cases} 2\sigma^2\,\tau\,t_0 - \sigma^2\,\tau^2(1 - e^{-\frac{t_0}{\tau}} - e^{-\frac{t_1}{\tau}} + e^{-\frac{\Delta t}{\tau}}) \\ \qquad \text{for } t_0 \le t_1,\ \Delta t = t_1 - t_0, \\ \qquad\qquad n_0 = n_1 = 1, \\[2mm] 0 \qquad \text{otherwise.} \end{cases} \tag{A.8b}$$

From these, one can construct the one-dimensional and multidimensional characteristic functions for $\tilde{w}(t)$:

$$\tilde{G}(s,t) = \exp[(is)^2\,\{\sigma^2\,\tau\,t - \sigma^2\,\tau^2\,(1 - e^{-\frac{t}{\tau}})\}], \tag{A.9a}$$

$$\tilde{G}(s_0, t_0; s_1, t_1)$$
$$= \exp[(is_0)\,(is_1)\,\{2\sigma^2\,\tau\,t_0 - \sigma^2\,\tau^2\,(1 - e^{-\frac{t_0}{\tau}} - e^{-\frac{t_1}{\tau}} + e^{-\frac{\Delta t}{\tau}})\}$$
$$+ (is_0)^2\,\{\sigma^2\,\tau\,t_0 - \sigma^2\,\tau^2\,(1 - e^{-\frac{t_0}{\tau}})\}$$
$$+ (is_1)^2\,\{\sigma^2\,\tau\,t_1 - \sigma^2\,\tau^2\,(1 - e^{-\frac{t_1}{\tau}})\}], \tag{A.9b}$$

which in turn allows deducing the one-dimensional and multidimensional moments of the integrated OU stochastic process:

$$\langle \tilde{w}^n(t) \rangle = \begin{cases} \frac{n!}{k!}\,\{\sigma^2\,\tau\,t - \sigma^2\,\tau^2(1 - e^{-\frac{t}{\tau}})\}^k & \text{for even } n = 2k, \\[2mm] 0 & \text{for odd } n, \end{cases} \tag{A.10a}$$

$$\langle \tilde{w}^{n_0}(t_0)\,\tilde{w}^{n_1}(t_1) \rangle = n_0!\,n_1! \sum_{m_1, m_2, m_3} \frac{1}{m_1!\,m_2!\,m_3!}$$
$$\times\, \{2\sigma^2\,\tau\,t_0 - \sigma^2\,\tau^2\,(1 - e^{-\frac{t_0}{\tau}} - e^{-\frac{t_1}{\tau}} + e^{-\frac{\Delta t}{\tau}})\}^{m_1} \tag{A.10b}$$
$$\times\, \{\sigma^2\,\tau\,t_0 - \sigma^2\,\tau^2\,(1 - e^{-\frac{t_0}{\tau}})\}^{m_2} \{\sigma^2\,\tau\,t_1 - \sigma^2\,\tau^2\,(1 - e^{-\frac{t_1}{\tau}})\}^{m_3}.$$

The sum in equation A.10b runs over all 3-tuple (m_1, m_2, m_3) obeying the conditions $m_1 + 2m_2 = n_0$ and $m_1 + 2m_3 = n_1$, that is, $m_1 + m_2 + m_3 = \frac{n_0+n_1}{2}$.

In the limit of a vanishing time constant, $\tau \to 0$, the integrated OU stochastic process $\tilde{w}(t)$ yields a Wiener-process $w(t)$ with one-dimensional and multidimensional cumulants:

$$\langle\langle w^n(t) \rangle\rangle = \begin{cases} 2Dt & \text{for } n = 2, \\ 0 & \text{otherwise,} \end{cases} \tag{A.11a}$$

$$\langle\langle w^{n_0}(t_0)\, w^{n_1}(t_1) \rangle\rangle = \begin{cases} 2D\min(t_0, t_1) & \text{for } n_0 = n_1 = 1, \\ 0 & \text{otherwise,} \end{cases} \tag{A.11b}$$

as well as one-dimensional and multidimensional moments:

$$\langle w^n(t) \rangle = \begin{cases} \frac{n!}{k!}(Dt)^k & \text{for even } n = 2k, \\ 0 & \text{for odd } n, \end{cases} \tag{A.12a}$$

$$\langle w^{n_0}(t_0)\, w^{n_1}(t_1) \rangle = n_0!\, n_1! \sum_{m_1, m_2, m_3} \frac{2^{m_1}}{m_1!\, m_2!\, m_3!} (D\,t_0)^{m_1+m_2} (D\,t_1)^{m_3}, \tag{A.12b}$$

where $D = \sigma^2\tau$. The sum in equation A.12b runs again over all 3-tuple (m_1, m_2, m_3) obeying $m_1 + m_2 + m_3 = \frac{n_0+n_1}{2}$.

A.3   The Itô Rules for the Integrated Ornstein-Uhlenbeck Stochastic Process. In the heart of the mathematical deduction of the Fokker-Planck equation from the Langevin equation 2.5 with colored noise sources lies a set of differential rules (Itô rules). It can be proved that for the integrated OU process $\tilde{w}(t)$, the Itô rules read:

$$d\tilde{w}_i(t)\, d\tilde{w}_j(t) = \delta_{ij} \left\{ \sigma^2\tau\, (1 - e^{-\frac{t}{\tau}}) + \frac{1}{2\tau}\, \tilde{w}_i^2(t) - \sigma^2 t \right\} dt, \tag{A.13a}$$

$$[d\tilde{w}(t)]^N = 0 \qquad \text{for } N \geq 3, \tag{A.13b}$$

$$[d\tilde{w}(t)]^N dt = 0 \qquad \text{for } N \geq 1, \tag{A.13c}$$

$$[dt]^N = 0 \qquad \text{for } N \geq 2. \tag{A.13d}$$

These rules apply for each of the three stochastic variables $\tilde{w}_{\{e,i\}}(t)$ and $\tilde{w}_I(t)$ obtained by integrating the OU processes $\tilde{g}_{\{e,i\}}(t)$ and $\tilde{I}(t)$, respectively (see section 2). Note that equation A.13a indicates that the independence of $\tilde{g}_{\{e,i\}}(t)$ and $\tilde{I}(t)$ directly translates into the independence between the corresponding integrated stochastic processes.

The rules A.13 have to be interpreted in the context of integration. Here, the integral $S(t) = \int_0^t d\eta(s)G(s)$ over a stochastic variable $\eta(t)$, where $G(t)$

denotes an arbitrary nonanticipating function or stochastic process, is approximated by the sum

$$S^\alpha(t) = \text{ms-lim}_{n\to\infty} S_n^\alpha(t), \tag{A.14a}$$

$$S_n^\alpha(t) = \sum_{k=1}^{n} G((1-\alpha)\,t_{k-1} + \alpha t_k)\,(\eta(t_k) - \eta(t_{k-1})), \tag{A.14b}$$

which evaluates the integral at n discrete time steps $t_k = k\frac{t}{n}$ in the interval $[0, t]$. The mean square limit ms-$\lim_{n\to\infty}$ is defined by the following condition of convergence: $S^\alpha(t) = \text{ms-lim}_{n\to\infty} S_n^\alpha(t)$ if and only if

$$\lim_{n\to\infty} \langle (S_n^\alpha(t) - S^\alpha(t))^2 \rangle = 0.$$

Note the dependence of this definition on the parameter α, which allows choosing the position in the interval $[t_{k-1}, t_k]$ where $G(t)$ is evaluated. In contrast to ordinary calculus, stochastic integrals in general do not become independent of α in the limit $n \to \infty$.

There are two popular choices for the parameter α. $\alpha = 1/2$ defines the Stratonovich calculus, which exhibits the same integration rules as ordinary calculus and is a common choice for integrals with stochastic variables describing noise with finite correlation time. However, mathematical strict proofs are nearly impossible to perform in the Stratonovich calculus. For instance, the Itô rules listed above can be derived only for $\alpha = 0$, which defines the Itô calculus. On the level of stochastic differential equations, a transformation between Itô and Stratonovich calculus can be shown. We will use this transformation to apply the Itô rules, which hold in the Itô calculus, to the Langevin equation, which allows a physical interpretation and treatment in the context of standard calculus only in the framework of the Stratonovich interpretation (see appendix 6.3). For more details about both stochastic calculi and their relation, we refer to standard textbooks of stochastic calculus (e.g., Gardiner, 2002).

Appendix B: Deduction of the Fokker-Planck Equation for the Stochastic Passive Membrane Equation

In this appendix we briefly outline the mathematical path we followed in deducing the Fokker-Planck equation for the passive membrane equation 2.1. For more details we refer to standard textbooks of stochastic calculus (e.g., Gardiner, 2002).

B.1 Itô's Formula for the Langevin Equation 2.5. In order to obtain the steady-state probability distribution of the membrane potential $V(t)$ for the Langevin equation with three independent multiplicative and additive colored noise terms (see equation 2.5), we first deduce Itô's formula for the

stochastic differential equation in question. Equation 2.5 together with the definition of the integrated OU stochastic process (see equation A.7) yields

$$\int_{V(0)}^{V(t)} dV(s) = \int_0^t ds\, f(V(s)) + \int_0^t d\tilde{w}_e(s)\, h_e(V(s))$$

$$+ \int_0^t d\tilde{w}_i(s)\, h_i(V(s)) + \int_0^t d\tilde{w}_I(s)\, h_I. \tag{B.1}$$

The first term on the right-hand side denotes the ordinary Riemannian integral over the drift term $f(V(t))$ given by equation 2.7, whereas the last three terms are stochastic integrals in the sense of Riemann-Stieltjes. This interpretation does not require the stochastic processes $\tilde{g}_{\{e,i\}}(t)$ and $\tilde{I}(t)$ to be gaussian white noise processes. Only the mathematically much weaker assumption that the corresponding integrated processes $\tilde{w}_{\{e,i\}}(t)$ and $\tilde{w}_I(t)$ are continuous function of t is required. This condition is fulfilled in the case of OU stochastic processes we consider here.

The natural choice for an interpretation of stochastic integral equations involving noise with finite correlation time is provided within the Stratonovich calculus (Mortensen, 1969; van Kampen, 1981; Gardiner, 2002). However, in order to solve the integral equation B.1 in a mathematically satisfying way by applying the Itô rules A.13 deduced in appendix 6.3, the integrals over stochastic variables in equation B.1 have to be written as Itô integrals (for a general discussion about the link between both Itô and Stratonovich interpretation, see, e.g., Gardiner, 2002). For instance, taking the defining equation A.14, the stochastic integral $S(t) = \int_0^t d\tilde{w}_e(s)\, h_e(V(s))$ has to be understood in the Stratonovich interpretation ($\alpha = \frac{1}{2}$) as

$$S(t) = \text{ms-lim}_{n\to\infty} \sum_{k=1}^n h_e(V(\tau_k))\, \{\tilde{w}_e(t_k) - \tilde{w}_e(t_{k-1})\}$$

$$= \text{ms-lim}_{n\to\infty} \left[\sum_{k=1}^n h_e(V(\tau_k))\, \{\tilde{w}_e(t_k) - \tilde{w}_e(\tau_k)\} \right.$$

$$\left. + \sum_{k=1}^n h_e(V(\tau_k))\, \{\tilde{w}_e(\tau_k) - \tilde{w}_e(t_{k-1})\} \right]. \tag{B.2}$$

Now we approximate $h_e(V(\tau_k))$, which is an analytic function of $V(t)$, by power expansion around the left point of the interval $[t_{k-1}, t_k]$. This yields in our case, where $h_e(V(\tau_k))$ is linear in $V(t)$, the linear function

$$h_e(V(\tau_k)) = h_e(V(t_{k-1})) + (\partial_V h_e(V(t_{k-1})))\,(V(\tau_k) - V(t_{k-1})). \tag{B.3}$$

Note that $h_e(V(\tau_k))$ does not explicitly depend on t.

To further resolve equation B.2, we remark that $V(t)$ is a solution of the stochastic Langevin equation 2.5, with an infinitesimal displacement given by

$$
\begin{aligned}
V(\tau_k) - V(t_{k-1}) = {} & f(V(t_{k-1}))\,(\tau_k - t_{k-1}) \\
& + h_e(V(t_{k-1}))\,(\tilde{w}_e(\tau_k) - \tilde{w}_e(t_{k-1})) \\
& + h_i(V(t_{k-1}))\,(\tilde{w}_i(\tau_k) - \tilde{w}_i(t_{k-1})) \\
& + h_I\,(\tilde{w}_I(\tau_k) - \tilde{w}_I(t_{k-1})).
\end{aligned}
\tag{B.4}
$$

Inserting this equation into equation B.3, and the result into the second sum of equation B.2, leaves us after a straightforward calculation with

$$
\begin{aligned}
S(t) = \text{ms-lim}_{n\to\infty} \Bigg[& \sum_{k=1}^{n} h_e(V(\tau_k))\,\{\tilde{w}_e(t_k) - \tilde{w}_e(\tau_k)\} \\
& + \sum_{k=1}^{n} (h_e(V(t_{k-1}))\,\{\tilde{w}_e(\tau_k) - \tilde{w}_e(t_{k-1})\} \\
& \qquad + 2\,\alpha_e(t_{k-1})\,\{\tau_k - t_{k-1}\}\,h_e(V(t_{k-1})) \\
& \qquad \times (\partial_V h_e(V(t_{k-1})))) \Bigg],
\end{aligned}
\tag{B.5}
$$

where

$$
2\,\alpha_e(t) = \sigma_e^2\,\tau_e\left(1 - \exp\left[-\frac{t}{\tau_e}\right]\right) + \frac{1}{2\,\tau_e}\,\tilde{w}_e^2(t) - \sigma_e^2\,t.
\tag{B.6}
$$

In order to obtain equation B.5, we made use of the fact that individual terms of the sum approximate integrals in the Itô calculus (equation A.14, $\alpha = 0$), which in turn allows the application of the Itô rules given in equation A.13.

For the third and fourth terms on the right-hand side of equation B.1, expressions similar to equations B.5 and B.6 can be obtained. Inserting the corresponding expressions in equation B.1 yields an infinitesimal displacement of the state variable $V(t)$:

$$
\begin{aligned}
dV(t) = {} & f(V(t))\,dt + h_e(V(t))\,d\tilde{w}_e(t) \\
& + h_i(V(t))\,d\tilde{w}_i(t) + h_I\,d\tilde{w}_I(t) \\
& + \alpha_e(t)\,h_e(V(t))\,\partial_V h_e(V(t))\,dt \\
& + \alpha_i(t)\,h_i(V(t))\,\partial_V h_i(V(t))\,dt,
\end{aligned}
\tag{B.7}
$$

where

$$2\,\alpha_{\{e,i,I\}}(t) = \sigma_{\{e,i,I\}}^2\,\tau_{\{e,i,I\}}\,\left(1 - \exp\left[-\frac{t}{\tau_{\{e,i,I\}}}\right]\right)$$
$$+ \frac{1}{2\,\tau_{\{e,i,I\}}}\,\tilde{w}_{\{e,i,I\}}^2(t) - \sigma_{\{e,i,I\}}^2\,t. \tag{B.8}$$

In deducing equation B.8 we made use of the fact that $h_{\{e,i\}}(V(t))$ are linear in $V(t)$ but do not explicitly depend on t (see equation 2.8a), whereas h_I (equation 2.8b) does not depend on $V(t)$ or t at all.

Denoting by $F(V(t))$ an arbitrary function of $V(t)$ satisfying equation B.8, an infinitesimal change of $F(V(t))$ with respect to $dV(t)$ is given by

$$dF(V(t)) = F(V(t) + dV(t)) - F(V(t))$$
$$= (\partial_V F(V(t)))\,dV(t)$$
$$+ \frac{1}{2}\,\left(\partial_V^2 F(V(t))\right)\,dV^2(t) + O(dV^3(t)), \tag{B.9}$$

where $O(dV^3(t))$ denotes terms of third or higher order in $dV(t)$. Substituting equation B.8 into equation B.9 and again applying the Itô rules A.13, we finally obtain Itô's formula,

$$dF(V(t)) = \partial_V F(V(t))\,f(V(t))\,dt + \partial_V F(V(t))\,h_e(V(t))\,d\tilde{w}_e(t)$$
$$+ \partial_V F(V(t))\,h_i(V(t))\,d\tilde{w}_i(t) + \partial_V F(V(t))\,h_I\,d\tilde{w}_I(t)$$
$$+ \partial_V F(V(t))\,\alpha_e(t)\,h_e(V(t))\,\partial_V h_e(V(t))\,dt$$
$$+ \partial_V F(V(t))\,\alpha_i(t)\,h_i(V(t))\,\partial_V h_i(V(t))\,dt$$
$$+ \partial_V^2 F(V(t))\,\alpha_e(t)\,h_e^2(V(t))\,dt + \partial_V^2 F(V(t))\,\alpha_i(t)\,h_i^2(V(t))\,dt$$
$$+ \partial_V F(V(t))\,h_I\,d\tilde{w}_I(t) + \partial_V^2 F(V(t))\,\alpha_I(t)\,h_I^2\,dt, \tag{B.10}$$

which describes an infinitesimal displacement of $F(V(t))$ as a function of infinitesimal changes in its variables. Note that equation B.10 shows that due to the dependence on stochastic variables, this displacement differs from those expected from ordinary calculus.

B.2 The Fokker-Planck Equation for the Langevin Equation 2.5. We now take the formal average of Itô's formula B.10:

$$\langle dF(V(t))\rangle = \langle \partial_V F(V(t))\,f(V(t))\,dt\rangle + \langle \partial_V F(V(t))\,h_e(V(t))\,d\tilde{w}_e(t)\rangle$$
$$+ \langle \partial_V F(V(t))\,h_i(V(t))\,d\tilde{w}_i(t)\rangle + \langle \partial_V F(V(t))\,h_I\,d\tilde{w}_I(t)\rangle$$
$$+ \langle \partial_V F(V(t))\,\alpha_e(t)\,h_e(V(t))\,\partial_V h_e(V(t))\,dt\rangle$$

$$+ \langle \partial_V F(V(t)) \, \alpha_i(t) \, h_i(V(t)) \, \partial_V h_i(V(t)) \, dt \rangle$$

$$+ \langle \partial_V^2 F(V(t)) \, \alpha_e(t) \, h_e^2(V(t)) \, dt \rangle$$

$$+ \langle \partial_V^2 F(V(t)) \, \alpha_i(t) \, h_i^2(V(t)) \, dt \rangle$$

$$+ \langle \partial_V F(V(t)) \, h_I \, d\tilde{w}_I(t) \rangle + \langle \partial_V^2 F(V(t)) \, \alpha_I(t) \, h_I^2 \, dt \rangle, \quad \text{(B.11)}$$

which yields

$$\left\langle \frac{dF(V(t))}{dt} \right\rangle = \langle \partial_V F(V(t)) \, f(V(t)) \rangle$$

$$+ \langle \partial_V F(V(t)) \, \alpha_e(t) \, h_e(V(t)) \, \partial_V h_e(V(t)) \rangle$$

$$+ \langle \partial_V F(V(t)) \, \alpha_i(t) \, h_i(V(t)) \, \partial_V h_i(V(t)) \rangle$$

$$+ \langle \partial_V^2 F(V(t)) \, \alpha_e(t) \, h_e^2(V(t)) \rangle$$

$$+ \langle \partial_V^2 F(V(t)) \, \alpha_i(t) \, h_i^2(V(t)) \rangle$$

$$+ \langle \partial_V^2 F(V(t)) \, \alpha_I(t) \, h_I^2 \rangle. \quad \text{(B.12)}$$

In the last step, we used the fact that $h_{\{e,i,I\}}$ are nonanticipating functions and, thus, are statistically independent of $d\tilde{w}_{\{e,i,I\}}$, respectively. Furthermore, we made use of $\langle d\tilde{w}(t) \rangle = \langle \tilde{g}(t) dt \rangle \equiv 0$ for the integrated OU process.

Defining the average (or expectation value) of the arbitrary function $F(V(t))$ as

$$\langle F(V(t)) \rangle = \int dV(t) \, F(V) \, \rho(V, t), \quad \text{(B.13)}$$

where $\rho(V, t)$ denotes the probability density function with finite support in the space of the state variable $V(t)$, we have

$$\frac{d}{dt} \langle F(V(t)) \rangle = \left\langle \frac{dF(V(t))}{dt} \right\rangle. \quad \text{(B.14)}$$

Performing the time derivative on the right-hand side of equation B.13 yields, after inserting equation B.12 and partial integration, the Fokker-Planck equation of the passive membrane equation with multiplicative and additive noise sources:

$$\partial_t \rho(V, t) = -\partial_V (f(V(t)) \, \rho(V, t))$$

$$+ \partial_V (h_e(V(t)) \, \partial_V (h_e(V(t)) \, \alpha_e(t) \rho(V, t)))$$

$$+ \partial_V (h_i(V(t)) \, \partial_V (h_i(V(t)) \, \alpha_i(t) \rho(V, t)))$$

$$+ h_I^2 \, \alpha_I(t) \, \partial_V^2 \rho(V, t), \quad \text{(B.15)}$$

where

$$
2\alpha_{\{e,i,I\}}(t) = \sigma^2_{\{e,i,I\}} \tau_{\{e,i,I\}} \left(1 - \exp\left[-\frac{t}{\tau_{\{e,i,I\}}}\right]\right)
$$
$$
+ \frac{1}{2\tau_{\{e,i,I\}}} \langle \tilde{w}^2_{\{e,i,I\}}(t) \rangle - \sigma^2_{\{e,i,I\}} t.
$$

Acknowledgments

References

Azouz, R., & Gray, C. (1999). Cellular mechanisms contributing to response variability of cortical neurons in vivo. *J. Neurosci., 19*, 2209–2223.

Baranyi, A., Szente, M. B., & Woody, C. D. (1993a). Electrophysiological characterization of different types of neurons recorded in vivo in the motor cortex of the cat. I. Patterns of firing activity and synaptic responses. *J. Neurophysiol., 69*, 1850–1864.

Baranyi, A., Szente, M. B., & Woody, C. D. (1993b). Electrophysiological characterization of different types of neurons recorded in vivo in the motor cortex of the cat. II. Membrane parameters, action potentials, current-induced voltage responses and electrotonic structures. *J. Neurophysiol., 69*, 1865–1879.

Barrett, J. N. (1975). Motoneuron dendrites: Role in synaptic integration. *Fed. Proc., 34*, 1398–1407.

Benzi, R., Suter, A., & Vulpiani, A. (1981). The mechanism of stochastic resonance. *J. Phys., A14*, L453–L457.

Bernander, Ö., Douglas, R. J., Martin, K. A. C., & Koch, C. (1991). Synaptic background activity influences spatiotemporal integration in single pyramidal cells. *Proc. Natl. Acad. Sci. USA, 88*, 11569–11573.

Bindman, L. J., Meyer, T., & Prince, C. A. (1988). Comparison of the electrical properties of neocortical neurones in slices in vitro and in the anaesthetized rat. *Exp. Brain Res., 69*, 489–496.

Borg-Graham, L. J., Monier, C., & Frégnac, Y. (1998). Visual input evokes transient and strong shunting inhibition in visual cortical neurons. *Nature, 393*, 369–373.

Brunel, N., Chance, F. S., Fourcaud, N., & Abbott, L. F. (2001). Effects of synaptic noise and filtering on the frequency response of spiking neurons. *Phys. Rev. Lett., 86*, 2186–2189.

Burkitt, A. N., & Clark, G. M. (2001). Synchronization of the neural response to noisy periodic synaptic input. *Neural Comp., 13*, 2639–2672.

Calvin, W. H., & Stevens, C. F. (1968). Synaptic noise and other sources of randomness in motoneuron interspike intervals. *J. Neurophysiol., 31*, 574–587.

Chance, F. S., Abbott, L. F., & Reyes, A. D. (2002). Gain modulation from background synaptic input. *Neuron, 35*, 773–782.

Contreras, D., Timofeev, I., & Steriade, M. (1996). Mechanisms of long lasting hyperpolarizations underlying slow sleep oscillations in cat corticothalamic networks. *J. Physiol., 494*, 251–264.

Cox, D. R., & Lewis, P. A. W. (1966). *The statistical analysis of series of events*. London: Methuen.

Cragg, B. G. (1967). The density of synapses and neurones in the motor and visual areas of the cerebral cortex. *J. Anat., 101*, 639–654.

DeFelipe, J., & Fariñas, I. (1992). The pyramidal neuron of the cerebral cortex: Morphological and chemical characteristics of the synaptic inputs. *Prog. Neurobiol., 39*, 563–607.

De Groff, D., Neelakanta, P. S., Sudhakar, R., & Aalo, V. (1993). Stochastical aspects of neuronal dynamics: Fokker-Planck approach. *Biol. Cybern., 69*, 155–164.

Destexhe, A., Mainen, Z. F., & Sejnowski, T. J. (1998). Kinetic models of synaptic transmission. In C. Koch & I. Segev (Eds.), *Methods in neuronal modeling* (2nd ed., pp. 1–26). Cambridge, MA: MIT Press.

Destexhe, A., & Paré, D. (1999). Impact of network activity on the integrative properties of neocortical pyramidal neurons in vivo. *J. Neurophysiol., 81*, 1531–1547.

Destexhe, A., Rudolph, M., Fellous, J.-M., & Sejnowski, T. J. (2001). Fluctuating synaptic conductances recreate in vivo-like activity in neocortical neurons. *Neuroscience, 107*, 13–24.

Doiron, B., Longtin, A., Berman, N., & Maler, L. (2000). Subtractive and divisible inhibition: Effect of voltage-dependent inhibitory conductances and noise. *Neural Comp., 13*, 227–248.

Érdi P. (1994). Noise and chaos in neural systems. In F. Ventriglia (Ed.), *Neural modeling and neural networks* (pp. 163–184). New York: Pergamon Press.

Evarts, E. V. (1964). Temporal patterns of discharge of pyramidal tract neurons during sleep and waking in the monkey. *J. Neurophysiol., 27*, 152–171.

Feller, W. (1951). Diffusion equations in genetics. In *Proceedings of the Second Berkeley Symposium on Mathematical Statistics and Probability* (pp. 227–246). Berkeley: University of California Press.

Fellous, J.-M., Rudolph, M., Destexhe, A., & Sejnowski, T. J. (in press). Variance detection and gain modulation in an in vitro model of in vivo activity. *Neuroscience*.

Gammaitoni, L., Hänggi, P., Jung, P., & Marchesoni, F. (1998). Stochastic resonance. *Rev. Mod. Phys., 70*, 223–287.

Gardiner, C. W. (2002). *Handbook of stochastic methods*. Berlin: Springer-Verlag.

Genovese, W., & Muñoz, M. A. (1999). Recent results on multiplicative noise. *Phys. Rev. E, 60*, 69–78.

Gillespie, D. T. (1996). The mathematics of Brownian motion and Johnson noise. *Am. J. Phys., 64*, 225–240.

Gruner, J. E., Hirsch, J. C., & Sotelo, C. (1974). Ultrastructural features of the isolated suprasylvian gyrus. *J. Comp. Neurol., 154*, 1–27.

Hänggi, P., & Jung, P. (1994). Colored noise in dynamical systems. *Adv. in Chem. Phys., 89*, 239–329.

Hillenbrand, U. (2002). Subthreshold dynamics of the neural membrane potential driven by stochastic synaptic input. *Phys. Rev. E, 66*, 021909–021920.

Hines, M. L., & Carnevale, N. T. (1997). The NEURON simulation environment. *Neural Computation, 9*, 1179–1209.

Hô, N., & Destexhe, A. (2000). Synaptic background activity enhances the responsiveness of neocortical pyramidal neurons. *J. Neurophysiol., 84*, 1488–1496.

Hodgkin, A. L., & Huxley, A. F. (1952). A quantitative description of membrane current and its application to conduction and excitation in nerve. *J. Physiol., 117*, 500–544.

Holmes, W. R., & Woody, C. D. (1989). Effects of uniform and non-uniform synaptic "activation-distributions" on the cable properties of modeled cortical pyramidal neurons. *Brain Res., 505*, 12–22.

Horsthemke, W., & Lefever, R. (1984). *Noise-induced transitions*. Berlin: Springer-Verlag.

Hubel, D. (1959). Single-unit activity in striate cortex of unrestrained cats. *J. Physiol., 147*, 226–238.

Huguenard, J. R., Hamill, O. P., & Prince, D. A. (1988). Developmental changes in Na^+ conductances in rat neocortical neurons: Appearance of a slow inactivating component. *J. Neurophysiol., 59*, 778–795.

Ibañes, M., García-Ojalvo, J., Toral, R., & Sancho, J. M. (1999). Noise-induced phase separation: Mean-field results. *Phys. Rev. E, 60*, 3597–3605.

Koch, C. (1999). *Biophysics of computation*. New York: Oxford University Press.

Koch, C., Bernander, Ö., & Douglas, R. J. (1995). Do neurons have a voltage or a current threshold for action potential initiation? *J. Comp. Neurosci., 2*, 63–82.

Kohn, A. F. (1997). Computer simulation of noise resulting from random synaptic activities. *Comput. Biol. Med., 27*, 293–308.

Lampl, I., Reichova, I., & Ferster, D. (1999). Synchronous membrane potential fluctuations in neurons of the cat visual cortex. *Neuron, 22*, 361–374.

Lánský, P., & Lánská, V. (1987). Diffusion approximation of the neuronal model with synaptic reversal potentials. *Biol. Cybern., 56*, 19–26.

Lánský, P., & Rodriguez, R. (1999). Two-compartment stochastic model of a neuron. *Physica, D 132*, 267–286.

Lánský, P., & Rospars, J. P. (1995). Ornstein-Uhlenbeck model neuron revisited. *Biol. Cybern., 72*, 397–406.

Lánský, P., Sacerdote, L., & Tomassetti, F. (1995). On the comparison of Feller and Ornstein-Uhlenbeck models for neural activity. *Biol. Cybern., 73*, 457–465.

Lapicque, L. (1907). Recherches quantitatives sur l'excitation électrique des nerfs traitée comme une polarization. *J. Physiol. Pathol. Gen., 9*, 620–635.

Levitan, H., Segundo, J. P., Moore, G. P., & Perkel, D. H. (1968). Statistical analysis of membrane potential fluctuations. *Biophys. J., 8*, 1256–1274.

Longtin, A. (2000). Effect of noise on the tuning properties of excitable systems *Chaos, Solitons and Fractals, 11*, 1835–1848.

Manwani, A., & Koch, C. (1999a). Detecting and estimating signals in noisy cable structure, I: Neuronal noise sources. *Neural Comput., 11*, 1797–1829.

Manwani, A., & Koch, C. (1999b). Detecting and estimating signals in noisy cable structures, II: Information theoretical analysis. *Neural Comput., 11*, 1831–1873.

Matsumura, M., Cope, T., & Fetz, E. E. (1988). Sustained excitatory synaptic input to motor cortex neurons in awake animals revealed by intracellular recording of membrane potentials. *Exp. Brain Res., 70*, 463–469.

Mauro, A., Conti, F., Dodge, F., & Schor, R. (1970). Subthreshold behavior and phenomenological impedance of the squid giant axon. *J. Gen. Physiol., 55*, 497–523.

Mortensen, R. E. (1969). Mathematical problems of modeling stochastic nonlinear dynamical systems. *J. Stat. Phys., 1*, 271–296.

Nicolis, C. (1982). Stochastic aspects of climatic transitions—response to a periodic forcing. *Tellus, 34*, 1–9

Nowak, L. G., Sanchez-Vives, M. V., & McCormick, D. A. (1997). Influence of low and high frequency inputs on spike timing in visual cortical neurons. *Cereb. Cortex, 7*, 487–501.

Paré, D., Shink, E., Gaudreau, H., Destexhe, A., & Lang, E. J. (1998). Impact of spontaneous synaptic activity on the resting properties of cat neocortical neurons in vivo. *J. Neurophysiol., 79*, 1450–1460.

Poliakov, A. V., Powers, R. K., Sawczuk, A., & Binder, M. D. (1996). Effects of background noise on the response of rat and cat motoneurones to excitatory current transients. *J. Physiol., 495*, 143–157.

Poznanski, R. R., & Peiris, M. S. (1996). Subthreshold response to white-noise current input in a tapering cable model of a neuron. *J. Math. Appl. Med. Biol., 13*, 207–222.

Prescott, S. A., & De Koninck, Y. (2003). Gain control of firing rate by shunting inhibition: Roles of synaptic noise and dendritic saturation. *Proc. Natl. Acad. Sci. USA, 100*, 2076–2081.

Rapp, M., Yarom, Y., & Segev, I. (1992). The impact of parallel fiber background activity on the cable properties of cerebellar Purkinje cells. *Neural Comp., 4*, 518–533.

Regehr, W. G., & Stevens, C. F. (2001). Physiology of synaptic transmission and short-term plasticity. In W. M. Cowan, T. C. Südhof, & C. F. Stevens (Eds.), *Synapses* (pp. 135–175). Baltimore: John Hopkins University Press.

Ricciardi, L. M., & Sacerdote, L. (1979). The Ornstein-Uhlenbeck process as a model for neuronal activity. I. Mean and variance of the firing time. *Biol. Cybern., 35*, 1–9.

Risken, H. (1984). *The Fokker Planck equation: Methods of solution and application*. Berlin: Springer-Verlag.

Rudolph M., & Destexhe A. (2001a). Correlation detection and resonance in neural systems with distributed noise sources. *Phys. Rev. Lett., 86*, 3662–3665.

Rudolph M., & Destexhe A. (2001b). Do neocortical pyramidal neurons display stochastic resonance? *J. Comp. Neurosci., 11*, 19–42.

Rudolph, M., & Destexhe, A. (2002). Gain modulation and frequency locking under conductance noise. *Neurocomputing, 52–54*, 907–912.

Rudolph, M., & Destexhe, A. (2003). A fast-conducting, stochastic integrative mode for neocortical neurons in vivo. *J. Neurosci., 23*, 2466–2476.

Rudolph, M., Hô, N., & Destexhe, A. (2001). Synaptic background activity affects the dynamics of dendritic integration in model neocortical pyramidal neurons. *Neurocomp., 38–40*, 327–333.

Salinas, E., & Sejnowski, T. J. (2000). Impact of correlated synaptic input on output firing rate and variability in simple neuronal models. *J. Neurosci., 20*, 6193–6209.

Stein, R. B. (1967). Some models of neuronal variability. *Biophys. J., 7*, 37–68.

Steriade, M. (1978). Cortical long-axoned cells and putative interneurons during the sleep-waking cycle. *Behav. Brain Sci., 3*, 465–514.

Steriade, M., Timofeev, I., & Grenier, F. (2001). Natural waking and sleep states: A view from inside neocortical neurons. *J. Neurophysiol., 85*, 1969–1985.

Szentagothai, J. (1965). The use of degeneration in the investigation of short neuronal connections. In M. Singer & J. P. Shade (Eds.), *Progress in brain research, 14* (pp. 1–32). Amsterdam: Elsevier.

Tiesinga, P. H. E., José, J. V., & Sejnowski, T. J. (2000). Comparison of current-driven and conductance-driven neocortical model neurons with Hodgkin-Huxley voltage-gated channels. *Phys. Rev. E 62*, 8413–8419.

Traub, R. D., & Miles, R. (1991). *Neuronal networks of the hippocampus*. Cambridge: Cambridge University Press.

Traynelis, S. F., & Jaramillo F. (1998). Getting the most out of noise in the central nervous system. *Trends Neurosci., 21*, 137–145.

Tuckwell, H. C. (1988). *Introduction to theoretical neurobiology*. Cambridge: Cambridge University Press.

Tuckwell, H. C., & Walsh, J. B. (1983). Random currents through nerve membranes. I. Uniform Poisson or white noise current in one-dimensional cables. *Biol. Cybern., 49*, 99–110.

Tuckwell, H. C., Wan, F. Y. M., & Rospars, J.-P. (2002). A spatial stochastic neuronal model with Ornstein-Uhlenbeck input current. *Biol. Cybern., 86*, 137–145.

Tuckwell, H. C., Wan, F. Y. M., & Wong, Y. S. (1984). The interspike interval of a cable model neuron with white noise input. *Biol. Cybern., 49*, 155–167.

Uhlenbeck, G. E., & Ornstein, L. S. (1930). On the theory of the Brownian motion. *Phys. Rev., 36*, 823–841.

Van den Broeck, C., Parrondo, J. M. R., Armero, J., & Hernández-Machado, A. (1994). Mean field model for spatially extended systems in the presence of multiplicative noise. *Phys. Rev. E, 49*, 2639–2643.

Van den Broeck, C., Parrondo, J. M., & Toral, R. (1994). Noise-induced nonequilibrium phase transition. *Phys. Rev. Lett., 73*, 3395–3398.

van Kampen, N. G. (1981). *Stochastic processes in physics and chemistry*. Amsterdam: North-Holland.

van Rossum, M. C. W. (2001). The transient precision of integrate and fire neurons: Effect of background activity and noise. *J. Comp. Neurosci., 10*, 303–311.

Volgushev, M., & Eysel, U. T. (2000). Noise makes sense in neuronal computing. *Science, 290*, 1908.

Wang, M. C., & Uhlenbeck, G. E. (1945). On the theory of Brownian motion II. *Rev. Mod. Phys., 17*, 323–342.

Werner, M. J., & Drummond, P. D. (1997). Robust algorithms for solving stochastic partial differential equations. *J. Comp. Phys., 132*, 312–326.

White, J. A., Rubinstein, J. T., & Kay, A. R. (2000). Channel noise in neurons. *Trends in Neurosci., 23*, 131–137.